

The temporal dimension of differenced Normalized Burn Ratio (dNBR) fire/burn severity studies: the case of the large 2007 Peloponnese wildfires in Greece

S. VERAVERBEKE\*<sup>†</sup>, S. LHERMITTE<sup>‡</sup>, W.W. VERSTRAETEN<sup>§</sup> AND R. GOOSSENS<sup>†</sup>

<sup>†</sup> Department of Geography, Ghent University, Ghent, Belgium

<sup>‡</sup> Centro de Estudios Avanzados en Zonas Aridas (CEAZA), Universidad de la Serena, La Serena, Chile

<sup>§</sup> Geomatics Engineering, Katholieke Universiteit Leuven (K.U.Leuven), Leuven, Belgium

\*Corresponding author. Email: sander.veraverbeke@ugent.be

## Abstract

The temporal dimension of differenced Normalized Burn Ratio (dNBR) fire/burn severity studies was studied for the case of the large 2007 Peloponnese wildfires in Greece. Fire severity is defined as the degree of environmental change as measured immediately post-fire, whereas burn severity combines the direct fire impact and ecosystems responses. Geo Composite Burn Index (GeoCBI), two pre-/post-fire differenced Thematic Mapper (TM) dNBR assessments and a Moderate Resolution Imaging Spectroradiometer (MODIS) dNBR time series were used to analyze the temporal dimension. MODIS dNBR time series were calculated based on the difference between the NBR of the burned and control pixels, which were retrieved using time series similarity of a pre-fire year. The analysis incorporated the optimality statistic, which evaluates index performance based on displacements in the mid-infrared-near infrared bi-spectral space. Results showed a higher correlation between field and TM data early post-fire ( $R^2 = 0.72$ ) than one year post-fire ( $R^2 = 0.56$ ). Additionally, mean

dNBR (0.56 vs. 0.29), the dNBR standard deviation (0.29 vs. 0.19) and mean optimality (0.65 vs. 0.47) were clearly higher for the initial assessment than for the extended assessment. This is due to regenerative processes that obscured first-order fire effects impacting the suitability of the dNBR to assess burn severity in this case study. This demonstrates the importance of the lag timing, i.e. time since fire, of an assessment, especially in a quickly recovering Mediterranean ecosystem. The MODIS time series was used to study intra-annual changes in index performance. The seasonal timing of an assessment highly impacts what is actually measured. This seasonality affected both the greenness of herbaceous resprouters and the productivity of the control pixels, which is land cover specific. Appropriate seasonal timing of an assessment is therefore of paramount importance to anticipate false trends (e.g. caused by senescence). Although these findings are case study specific, it can be expected that similar temporal constraints affect assessments in other ecoregions. Therefore, within the limitations of available Landsat imagery, caution is recommended for the temporal dimension when assessing post-fire effects. This is crucial, especially for studies that aim to evaluate trends in fire/burn severity across space and time. Also, clarification in associated terminology is suggested.

## 1 Introduction

Wildfires affect the ecological functioning of many ecosystems (Dwyer et al., 1999; Pausas, 2004; Riano et al., 2007) as they partially or completely remove the vegetation layer and affect post-fire vegetation composition (Epting and Verbyla, 2005; Lentile et al., 2005). They act as a natural component in vegetation succession cycles (Trabaud, 1981; Capitaino and Carcaillet, 2008; Roder et al., 2008) but also potentially increase degradation processes, such as soil erosion (Thomas et al., 1999; Perez-Cabello et al., 2006; Chafer, 2008; Fox et al., 2008). Assessment of post-fire effects is thus a major challenge to understand the potential degradation after fire (Kutiel and Inbar, 1993; Fox et al., 2008) and to comprehend the ecosystem's post-fire resilience (Epting and Verbyla, 2005; Lentile et al., 2005).

The fire impact can be described as (i) the amount of damage (Hammill and Bradstock, 2006; Gonzalez-Alonso et al., 2007; Chafer, 2008), (ii) the physical, chemical and biological changes (Landmann, 2003; Chafer et al., 2004; Cocke et al., 2005; Stow et al., 2007; Lee et al., 2008) or (iii) the degree of alteration (Brewer et al., 2005; Eidenshink et al., 2007) that fire causes to an ecosystem and is quantified as the severity of fire. In this context the terms fire severity and burn severity are often interchangeably used (Keeley, 2009). Lentile et al. (2006), however, suggest a clear distinction between both terms by considering the disturbance continuum (Jain et al., 2004), which addresses three different temporal fire effects phases: before, during and after the fire. In this framework fire severity quantifies the short-term fire effects in the immediate post-fire environment while burn severity quantifies both the short- and long-term impact as it includes response processes. While this substantive difference in terminology between fire and burn severity is generally accepted in the remote sensing community, fire ecologists tend to smooth away this distinction as they opt to exclude ecosystem responses from the term burn severity (Keeley, 2009), thereby reducing its meaning to the same dimension as the term fire severity, which makes both terms mutually

substitutional. However, the inclusion of ecosystem responses (such as regrowth, regeneration and resilience) in burn severity is justified by the significant negative correlation between direct fire impact and regeneration ability (Diaz-Delgado et al., 2003). Moreover, except for assessments immediately post-fire (within the first month), ecosystem responses cannot be neglected in a satellite assessment as it is practically infeasible to uncouple these effects from the direct fire impact based on the image data. In addition, Key and Benson (2005) and Key (2006) introduced three sets of complementary concepts. The first set differentiates between first- and second-order effects, where first-order effects are caused by the fire only, whereas second-order effects also involve other causal agents (e.g. wind, rain, vegetative processes, etc.). Secondly, short- and long-term severity refer to the condition of the burned area. Short-term severity is restricted to the pre-recovery phase, while long-term severity includes both first- and second-order effects. Thirdly, Key (2006) differentiates between an initial assessment (IA) and an extended assessment (EA). This difference results from differing lag timing, i.e. the time since fire, on which an assessment is made. An IA is executed immediately after the fire event, whereas by EAs a certain amount of time elapses between the fire event and the assessment. Summarized, fire severity is defined as the degree of environmental change caused by fire and is related to first-order effects, short-term severity and IAs (Key and Benson, 2005). As such it mainly quantifies vegetation consumption and soil alteration. Burn severity, on the other hand, is equally defined as the degree of environmental change caused by fire, but it also includes second-order effects (e.g. resprouting, delayed mortality, etc.), long-term severity and is usually measured in an EA (Key and Benson, 2005). Finally, the term post-fire effects (Lentile et al., 2006) groups all above mentioned severity-related notions. In figure 1 a schematic representation of post-fire effects terminology is given.

Even though a considerable amount of remote sensing studies have focused on the use of the Normalized Difference Vegetation Index (NDVI) for assessing burn severity (Isaev et al., 2002; Diaz-Delgado et al., 2003; Ruiz-Gallardo et al., 2004; Chafer et al., 2004; Hammill and Bradstock, 2006; Hudak et al., 2007), the Normalized Burn Ratio (NBR) has become accepted as the standard spectral index to estimate fire/burn severity (e.g. Lopez-Garcia and Caselles, 1991; Epting et al., 2005; Key and Benson, 2005; Bisson et al., 2008; Veraverbeke et al., 2010ab). The NBR is used as an operational tool at national scale in the United States (Eidenshink et al., 2007). The index relates to vegetation vigor and moisture by combining near infrared (NIR) and mid infrared (MIR) reflectance and is defined as:

$$NBR = \frac{NIR - MIR}{NIR + MIR} \quad (1)$$

Most of the studies that assessed burn severity were conducted with Landsat imagery (French et al., 2008), thanks to Landsat's unique properties of operating a MIR band and a desirable 30 m resolution for local scale studies. Since fire effects on vegetation produce a reflectance increase in the MIR spectral region and a NIR reflectance drop (Pereira et al., 1999; Key, 2006), bi-temporal image differencing is frequently applied on pre- and post-fire NBR images resulting in the differenced Normalized Burn Ratio (dNBR) (Key and Benson, 2005). Additionally, Miller and Thode (2007) proposed a relative version of the dNBR (RdNBR). This index takes into account the pre-fire amount of biomass, and therefore, rather than being a measure of absolute change, reflects the change caused by fire relative to the pre-fire condition. Apart from the correlation with field data (Key and Benson, 2005; De Santis and Chuvieco, 2009; Veraverbeke et al., 2010ab), the performance of bi-spectral indices can be evaluated by assessing a pixel's shift in the bi-spectral feature space. As such, a pixel-based optimality measure, originating from the spectral index theory (Verstraete and Pinty, 1996), has been developed by Roy et al. (2006). They used the optimality concept to question the

dNBR method as an optimal fire/burn severity approach. The optimality value varies between zero (not at all optimal) and one (fully optimal). An optimal fire/burn severity spectral index needs to be as insensitive as possible to perturbing factors, such as atmospheric and illumination effects (Veraverbeke et al., 2010c), and highly sensitive to fire-induced vegetation changes.

These post-fire vegetation changes typically are abrupt immediately after fire (Pereira et al., 1999), whereas a more gradual and progressive vegetation regeneration process is initiated several weeks after the fire (Viedma et al., 1997; Pausas et al., 2004; Keeley et al., 2005; van Leeuwen, 2008). Despite of the current discussion on the temporal dimension in fire/burn severity studies (Keeley, 2009) (see figure 1), relatively few studies have addressed attention to the influence of assessment timing on the estimation of post-fire effects. In this respect Key (2006) comprehensively differentiates between two temporal constraints. The first constraint is the lag timing. IAs focus on the first opportunity to get an ecological evaluation of within-burn differences in combustion completeness, whereas EAs occur as a rule in the first post-fire growing season (Key, 2006). This constraint especially becomes obvious in quickly recovering ecosystems where an inappropriate lag timing can distort or hide the fire effects (Allen and Sorbel, 2008; Lhermitte et al. 2010a). Allen and Sorbel (2008), for example, found that IA and EA produced significantly different information for tundra vegetation, while the timing of the assessment had no effect for black spruce forest. This was attributed to the rapid tundra recovery (Allen and Sorbel, 2008). The second constraint deals with the seasonal timing, i.e. the biophysical conditions that vary throughout the year, regardless of the fire. Analysis shortly after the usually dry fire season for example can be detracted because of the reduced variability in vegetation vigor during the dry season. Conversely, when vegetation is green and productive, a broader range of severity can be detected with better contrast (Key, 2005). The importance of the phenological timing of an assessment was also pointed by

Verbyla et al. (2008). They found a clear discrepancy in dNBR values between two different Landsat assessments, which was partly attributed to the seasonal timing of the bi-temporal acquisition scheme, while another part of the difference was due to the changing solar elevation angles at the moment of the image acquisition. Apart from these studies, relatively little attention has been devoted to the temporal changes in the NBR and its consequence to estimate fire/burn severity. This is probably due to the 16-day repeat cycle of Landsat and the problem of cloudiness which restricts image availability to infrequent images over small areas (Ju and Roy, 2008). Multi-temporal Moderate Resolution Imaging Spectroradiometer (MODIS) data can bridge the gap of image availability. MODIS is the only high temporal-frequent coarse resolution (500 m) sensor which has the spectral capability, i.e. acquisition of reflectance data in the MIR region besides to the NIR region (Justice et al., 2002), to calculate the NBR. MODIS surface reflectance data (Vermote et al., 2002) are therefore an ideal source of information to explore the post-fire temporal, both in terms of lag and seasonal timing, sensitivity of the dNBR to assess fire/burn severity.

Hence, the general objective of this paper is assessing the temporal dimension of the dNBR and its consequence for the estimation of fire/burn severity of the large 2007 Peloponnese wildfires in Greece. This objective is fulfilled by evaluating (i) the relationship between field data of severity, Landsat dNBR and MODIS dNBR for an IA and EA scheme, and (ii) the one-year post-fire temporal changes in dNBR and dNBR optimality for different fuel types. 500 m MODIS dNBR data are used in this study as a way to explore the temporal dimension, not as a substitute for 30 m Landsat dNBR imagery which is superior for spatial detail (French et al. 2008).

## **2 Data and study area**

### **2.1 Study area**

The study area is situated at the Peloponnese peninsula, in southern Greece (36°30'-38°30' N, 21°-23° E) (see figure 2). The topography is rugged with elevations ranging between 0 and 2404 m above sea level. The climate is typically Mediterranean with hot, dry summers and mild, wet winter (see figure 3). For the Kalamata meteorological station (37°4' N, 22°1' E) the average annual temperature is 17.8°C and the mean annual precipitation equals 780 mm.

After a severe drought period several large wildfires of unknown cause have struck the area in August 2007. The fires consumed more than 150 000 ha of coniferous forest, broadleaved forest, shrub lands (maquis and phrygana communities) and olive groves. Black pine (*Pinus nigra*) is the dominant conifer species. Maquis communities consist of sclerophyllous evergreen shrubs of 2-3 m high (Polunin, 1980). Phrygana is dwarf scrub vegetation (< 1 m), which prevails on dry landforms (Polunin, 1980). The shrub layer is characterised by e.g. *Quercus coccifera*, *Q. frainetto*, *Pistacia lentiscus*, *Cistus salvifolius*, *C. incanus*, *Erica arborea*, *Sarcopoterum spinosum*. The olive groves consist of *Olea europaea* trees, whereas oaks are the dominant broadleaved species.

## 2.2 Field data

To assess fire/burn severity in the field, 150 Geo Composite Burn Index (GeoCBI) plots were collected one year post-fire, in September 2008 (see figure 2). The GeoCBI is a modified version of the Composite Burn Index (CBI) (De Santis and Chuvieco, 2009). The (Geo)CBI is an operational tool used in conjunction with the Landsat dNBR approach to assess fire/burn severity in the field (Key and Benson, 2005). The GeoCBI divides the ecosystem into five different strata, one for the substrates and four vegetation layers. These strata are: (i) substrates, (ii) herbs, low shrubs and trees less than 1 m, (iii) tall shrubs and trees of 1 to 5 m, (iv) intermediate trees of 5 to 20 m and (v) big trees higher than 20 m. In the field form, 20 different factors can be rated (e.g. soil and rock cover/color change, % LAI change, char height) (see table 1) but only those factors present and reliably rateable, are considered. The



186 rates are given on a continuous scale between zero and three and the resulting factor ratings  
187 are averaged per stratum. Based on these stratum averages, the GeoCBI is calculated in  
188 proportion to their corresponding fraction of cover, resulting in a weighted average between  
189 zero and three that expresses burn severity. As the field data were collected one year post-fire,  
190 it is an EA. To be able to explore the full temporal dimension of fire/burn severity these data  
191 were also used as an IA. This is justified as most of the rating factors are relatively stable in  
192 time (Key and Benson, 2005), and as such plot ratings would not significantly differ when IA  
193 and EA schemes would have been sampled independently. However, it is obvious to omit the  
194 factor new sprouts from the IA scheme as this factor is not relevant in a fire severity  
195 assessment (see figure 1).

196 The 150 sample points were selected based on a stratified sampling approach, taking into  
197 account the constraints on mainly accessibility and time, which encompasses the whole range  
198 of variation found within the burns. The field plots consist of 30 by 30 m squares, analogous  
199 to the Landsat pixel size. The pixel centre coordinates were recorded based on measurements  
200 with a handheld Garmin eTrex Vista Global Positioning System (15 m error in x and y  
201 (Garmin 2005)) device. To minimize the effect of potential misregistration, plots were at least  
202 90 m apart and chosen in relatively homogeneous areas (Key and Benson 2005). This  
203 homogeneity refers both to the fuel type (homogeneity of at least 500 m) and the fire effects  
204 (homogeneity of at least 60 m). Of the 150 field plots 63 plots were measured in shrub land,  
205 57 in coniferous forest, 16 in deciduous forest and 14 in olive groves. More information on  
206 the field sampling scheme can be found in Veraverbeke et al. (2010ab).

207 Additionally, 50 training samples in very homogeneous covers (homogeneity of at least  
208 2000m) were GPS-recorded outside the burned area (see figure 2). These samples comprised  
209 the most prevailing fuel types in the burned area; 12 samples were taken in coniferous forest,

17 in shrub land, 10 in deciduous forest and 11 in olive groves. The dominant species of these land cover types are given in section 2.1.

### **2.3 Landsat Thematic Mapper data**

For the traditional Landsat post-fire effects assessment of the summer 2007 Peloponnese fires three anniversary date Landsat Thematic Mapper (TM) images (path/row 184/34) were used (23/07/2006, 28/09/2007 and 13/08/2008). The images were acquired in the summer, minimizing effects of vegetation phenology and differing solar zenith angles. The images were subjected to geometric, radiometric, atmospheric and topographic correction.

The 2008 image was geometrically corrected using 34 ground control points (GCPs), recorded in the field with a Garmin eTrex Vista GPS. The resulting Root Mean Squared Error (RMSE) was lower than 0.5 pixels. The 2006, 2007 and 2008 images were co-registered within 0.5 pixels accuracy. All images were registered in UTM (Universal Transverse Mercator) (zone 34S), with WGS 84 (World Geodetic System 84) as geodetic datum.

Raw digital numbers (DNs) were scaled to at-sensor radiance values using the procedure of Chander et al. (2007). The radiance to reflectance conversion was performed using the COST method of Chavez (1996). The COST method is a dark object subtraction (DOS) approach that assumes 1% surface reflectance for dark objects (e.g. deep water). After applying the COST atmospheric correction, pseudo-invariant features (PIFs) such as deep water and bare soil pixels, were examined in the images. No further relative normalization between the images was required.

Additionally, it was necessary to correct for different illumination effects due to topography as the common assumption that shading effects are removed in ratio-based analyses does not necessarily hold true (Verbyla et al., 2008; Veraverbeke et al. 2010c). This was done based on the modified c-correction method (Veraverbeke et al. 2010c), a modification of the original c-correction approach (Teillet et al. 1982), using a digital elevation model (DEM) and

knowledge of the solar zenith and azimuth angle at the moment of image acquisition. Topographical slope and aspect data were derived from 90 m SRTM (Shuttle Radar Topography Mission) elevation data (Jarvis et al. 2006) resampled and co-registered with the TM images.

Finally, by inputting the NIR (TM4: centered at 830 nm) and MIR (TM7: centered at 2215 nm) bands in equation 1 NBR images were generated.

#### **2.4 Moderate Resolution Imaging Spectroradiometer data**

Level 2 daily Terra MODIS surface reflectance (500 m) tiles that cover the study area (MOD09GA) including associated Quality Assurance (QA) layers were acquired from the National Aeronautics and Space Administration (NASA) Warehouse Inventory Search Tool (WIST) (<https://wist.echo.nasa.gov>) for the period 01/01/2006 till 31/12/2008. These products contain an estimate of the surface reflectance for seven optical bands as it would have been measured at ground level as if there were no atmospheric scattering or absorption (Vermote et al., 2002). The data preprocessing steps included subsetting, reprojecting, compositing, creating continuous time series and indexing. The study area was clipped and the NIR (centered at 858 nm), MIR (centered at 2130 nm) and QA layers were reprojected into UTM with WGS 84 as geodetic datum. Subsequently, the daily NIR, MIR and QA data were converted in 8-day composites using the minimum NIR criterion to minimize cloud contamination and off-nadir viewing effects (Holben, 1986). The minimum NIR criterion has proven to allow a more accurate discrimination between burned and unburned pixels than traditional Maximum Value Composites (MVCs) (Barbosa et al., 1998; Stroppiana et al., 2002; Chuvieco et al., 2005). Thus, for each 8-day period the NIR, MIR and QA data were saved corresponding with the minimum NIR observation for each pixel. An additional advantage of the minimum NIR criterion in comparison with MVCs is its tendency to select close to nadir observations (Stroppiana et al., 2002), because for smaller view angles the soil

fraction in the vegetation-soil matrix will have a relatively higher contribution to the reflectance signal than for wider viewing angles. After the compositing procedure a minority of the data still lacked good quality values. Therefore, to create continuous time series, a local second-order polynomial function, also known as an adaptive Savitzky-Golay filter (Savitzky and Golay, 1964), was applied to the time series as implemented in the TIMESAT software (Jonsson and Eklundh, 2004) to replace the affected observations. Although other smoothing methods based on for example Fourier series (Olsson and Eklundh, 1994) or least-squares fitting to sinusoidal functions (Cihlar, 1996) are known to work well in most instances, they fail to capture a sudden steep change in remote sensing values, as it is the case in burned land applications (Verbesselt et al., 2006). The TIMESAT program allows the inclusion of a preprocessing mask. These masks are translated into weights, zero and one, that determine the uncertainty of the data values. Cloud-affected observations were identified using the QA layer and were assigned a zero weight value. Consequently these data do not influence the filter procedure. Only the values of the masked observations were replaced to retain as much as possible the original NIR and MIR reflectance values. Finally, NBR images were calculated based on equation 1.

### **3 Methodology**

#### **3.1 MODIS pre-fire land cover map**

As phenology, fire impact and regeneration typically vary by land cover type (Reed et al., 1994; White et al. 1996; Viedma et al. 1997) the pre-fire land cover of the burned areas was classified. This was done based on the time series similarity concept as phenological differences in time series allow to discriminate different land cover types (Reed et al., 1994; Viovy, 2000; Geerken et al., 2005, Lhermitte et al., 2008). A maximum likelihood classification was performed on a MODIS NBR time series of the pre-fire year 2006. The

GPS-recorded pixel and its bilinear neighbors of the 50 land cover field samples (see section 2.2 and figure 3) served as training pixels in the classification. As such the four main land covers (shrub land, coniferous forest, deciduous forest and olive groves) were classified. Figure 4 displays the mean temporal profiles of the training pixels for each class. Figures 4A-C, respectively of shrub land, coniferous forest and olive groves, reveal characteristic temporal profiles for evergreen Mediterranean species. For these land cover types seasonal fluctuations are minor. Coniferous forests are characterized by a higher overall productivity than shrub lands and olive groves. Shrub lands reveal a peak in late spring/early summer, which is characteristic for Mediterranean xerophytic species (Specht, 1981; Maselli, 2004). The olive groves are slightly more productive during the winter season, which can be contributed to the favorable moisture conditions during the wet winter months (see figure 3). The temporal profile of deciduous forest (figure 4D) contrasts with those of evergreen species as it shows a markedly higher seasonality with a summer maximum and winter minimum. The accuracy of the pre-fire land cover map was verified by the 150 GeoCBI field plots with known pre-fire land cover type.

### **3.2 MODIS control pixel selection**

Traditionally fire/burn severity is estimated from pre-/post-fire differenced imagery (Key and Benson, 2005; French et al., 2008). This bi-temporal analysis method can be hampered by phenological effects, both due to the differences in acquisition data and due to inter-annual meteorological variability (Diaz-Delgado and Pons, 2001). To deal with these phenological effects Diaz-Delgado and Pons (2001) proposed to compare vegetation regrowth in a burned area with unburned reference plots within the same image. As such, external and phenological variations are minimized among the compared areas. The reference plot selection procedure has, however, two main difficulties. Firstly, large scale application remains constrained due to the necessity of profound field knowledge to select relevant control plots. Secondly, the

reference plot approach fails to describe within-burn heterogeneity as it uses mean values per fire plot. To solve these problems, Lhermitte et al. (2010b) proposed a pixel-based control plot selection method which follows the same reasoning with respect to the minimization of phenological effects by comparison with image-based control plots. The difference with the reference plot procedure, however, is situated in the fact that the pixel-based method assigns a unique unburned control pixel to each burned pixel. This control pixel selection is based on the similarity between the time series of the burned pixel and the time series of its surrounding unburned pixels for a pre-fire year (Lhermitte et al., 2010b). The method allows to quantify the heterogeneity within a fire plot since each fire pixel is considered independently as a focal study pixel and a control pixel is selected from a contextual neighborhood around the focal pixel. In this study, the procedure of Lhermitte et al. (2010b) is followed as it allows exploring the temporal dimension of post-fire effects without image-to-image phenological constraints. The selection is based on the similarity of MODIS NBR time series between pixels during the pre-fire year 2006. The averaged Euclidian distance dissimilarity criterion  $D$  was used:

$$D = \frac{\sqrt{\sum_{t=1}^N (NBR_t^f - NBR_t^x)^2}}{N} \quad (2)$$

where  $NBR_t^f$  and  $NBR_t^x$  are the respective burned focal and unburned candidate control pixel time series, while  $N$  is the number of observations in pre-fire year ( $N=46$ ). The Euclidian distance metric has an intuitive appeal: it quantifies the straight line inter-point distance in a multi-temporal space as distance measure. As a result, it is robust for both data space translations and rotations. Consequently, it is a very useful metric to assess inter-pixel differences in time series (Lhermitte et al., 2010b). The discrimination between burned and unburned pixels was based on a burned area map. This burned area map was extracted making

use of the characteristic persistency of the post-fire NBR drop, similar to the algorithms of Kasischke and French (1995), Barbosa et al. (1999) and Chuvieco et al. (2008). To avoid possible confusion with harvested crop land a rough fire perimeter, approximately 1 km outside of the burned area, was manually digitized. Using the 8-day NBR composites as input, the dNBR between each single observation and its five consecutive observations in time was calculated ( $dNBR = NBR_t - NBR_{t+i}$  with  $i = 1, 2, 3, 4, 5$ ). When these five dNBR values all exceeded the threshold value of 0.125, the pixel was classified as burned. We have chosen a relatively low threshold to minimize the omission error on low severity pixels. The accuracy of the burned area map was verified using a TM-derived burned area map (Veraverbeke et al., 2010c).

For valid control plot estimates, control pixels must correspond to the focal pixel in case the fire had not occurred. Firstly, this implies identical pre-fire characteristics for both control and focal pixels. Secondly, it means similar post-fire environmental conditions. To determine the appropriate control pixel selection criteria, the method of Lhermitte et al. (2010b) was calibrated to our dataset. As we want to evaluate the control pixel selection procedure (based on pre-fire time series) after the fire event, an initial performance assessment is made on unburned pixels. Therefore 500 unburned pixels were randomly selected. For these pixels a fictive burning date was set at the same composite the real fire event took place.

Determining a number of control pixels  $c$  out of a number of candidate pixels  $x$ , which is related to window size, is essential for the selection procedure. Not only the most similar control pixel was considered because a beneficial averaging that removes random noise in the time series has been perceived in previous research (Lhermitte et al., 2010b). As a result the averaged time series of the two (or more) most similar pixel potentially provides better results. The calibration of the control pixel selection procedure requires an understanding of

how similarity is affected by varying window sizes and the number of selected control pixels. The sensitivity of dissimilarity criterion  $D$  was therefore assessed by comparing the outcome for varying number of control pixels ( $c = 1, 2, \dots, 15$ ) and varying window sizes ( $3 \times 3, 5 \times 5, \dots, 25 \times 25$ ). Evaluation consisted of measuring the temporal similarity for the 500 fictively burned sample pixel between  $NBR_t^f$  and  $NBR_t^x$  one year pre-fire and one year post-fire. For this purpose  $D$  was calculated between control and focal pixels for varying numbers of control pixels and varying window sizes. This allows to determine how well pre-fire similarity is maintained after a fictive burning date and how pre-/post-fire changes in similarity are related to the number of control pixels and window size.

Although this calibration experiment allows the determination of an optimal selection of  $c$  control pixels out of  $x$  candidate pixels, which is related to the window size, it does not fully take into account the spatial context of the actual burns. The calibration experiment is based on isolated pixels, while in reality burned areas consist of large patches. As a consequence in the calibration experiment the first eight candidate pixels are found in  $3 \times 3$ -window (nine pixels minus one burned pixel), while for finding eight candidate pixels for a burned pixel located in the middle of a large burn larger window sizes are required. As a result, the distance of the control pixels to their corresponding focal pixel is variable. This also implies that the performance of the procedure is likely to be better near the contours of the burn perimeter.

### 3.3 dNBR and optimality

After the derivation of preprocessed TM NBR images, these layers were bi-temporally differenced. This traditional bi-temporal differencing resulted in an IA and EA dNBR, respectively  $dNBR_{TM,IA}$  and  $dNBR_{TM,EA}$ :

$$dNBR_{TM,IA} = NBR_{TM,2006} - NBR_{TM,2007} \quad (3)$$



$$dNBR_{TM,EA} = NBR_{TM,2006} - NBR_{TM,2008} \quad (4)$$

Additionally, a MODIS dNBR time series was derived after differencing the respective focal ( $NBR_t^f$ ) and control ( $NBR_t^c$ ) images:

$$dNBR_t = NBR_t^c - NBR_t^f \quad (5).$$

Thus, in contrast with the traditional pre-/post-fire differencing as applied on the TM imagery, the MODIS dNBR was calculated based on focal and control pixels within the same image. For the same post-fire dates as with the TM dNBR images, the MODIS dNBR images were respectively labeled as  $dNBR_{MODIS,IA}$  and  $dNBR_{MODIS,EA}$ .

For evaluating the optimality of the bi-temporal change detection the MIR-NIR bi-spectral space was considered (see figure 5). If a spectral index is appropriate to the physical change of interest, in this case fire-induced vegetation depletion, there exists a clear relationship between the change and the direction of the displacement in the bi-spectral feature space (Verstraete and Pinty, 1996). In an ideal scenario a pixel's bi-temporal trajectory is perpendicular to the first bisector of the Cartesian coordinate system. This is illustrated in figure 5 for the displacement from unburned (U) to optimally (O) sensed burned. Perturbing factors decrease the performance of the index. Then a pixel's displacement can be decomposed in a vector perpendicular to the first bisector and a vector along the post-fire NBR isoline to which the index is insensitive. For example, in figure 5, a pixel shifts from unburned (U) to burned (B) after fire. Here, the magnitude of change to which the index is insensitive is equal to the Euclidian distance  $|OB|$ . Thus the observed displacement vector UB can be decomposed in the sum of the vectors UO and OB, hence, following the expression of Roy et al. (2006) index optimality is defined as:

$$optimality = 1 - \frac{|OB|}{|UB|} \quad (3)$$

As  $|OB|$  can never be larger than  $|UB|$ , the optimality measure varies between zero and one. If the optimality measure equals zero, then the index is completely insensitive to the change of interest. An optimality score of one means that the index performs ideally.

### 3.4 Analysis method

Firstly, the accuracy of the land cover map and the calibration of the control pixel selection procedure are verified. Secondly, the analysis has focused on the correlation between field and TM data for an IA and EA. In addition descriptive dNBR and optimality statistics were compared. To justify the use of MODIS dNBR to explore the temporal dimension the correlation between downsampled TM and corresponding MODIS dNBR imagery is also calculated. Finally, MODIS dNBR and optimality time series for different land cover types are compared. Emphasis has been both on the importance of lag and seasonal timing of an assessment.

## 4 Results

### 4.1 MODIS pre-fire land cover map

Figure 6 displays the pre-fire land cover map derived based on the time series similarity concept. Shrub land was the most prevailing land cover type. 100 372 ha (56.65% of the burned area) were classified as shrub land. The class coniferous forest covered 37 096 ha (20.95% of the burned area) which was only slightly more than the olive groves class (34 555 ha, 19.50% of the burned area). A minority of the pixels were classified as deciduous forest (624 ha, 2.90%). The error matrix of the land cover map is tabulated in table 2. The overall accuracy of the classification equalled 73% and a Kappa coefficient of 0.60 was obtained. As the phenology of deciduous forest contrasts with those of evergreen land cover classes (see figure 4), this class obtained high producer's and user's accuracies of respectively 81% and

93%. The evergreen land cover classes revealed a higher time series similarity. As a result the cover classes were prone to higher omission and commission errors. These errors remained, however, acceptable. The classification of shrub land resulted in both a producer's and user's accuracy of 75%. The producer's accuracy of coniferous forest equalled 72%, which was slightly lower than its user's accuracy of 76%. Finally, the accuracy of olive groves class was the lowest (producer's and user's accuracy of respectively 64% and 47%).

## **4.2 MODIS control pixel selection**

TM imagery was used to validate the MODIS burned area map. The TM-derived burned area map was derived after applying a two-phase  $dNBR_{TM,IA}$  threshold algorithm that was validated using field reference data resulting in a detection probability of 80% and a probability of false alarm of 5% (Veraverbeke et al., 2010c). MODIS burned area statistics were extracted in windows of 10 by 10 km. These statistics were regressed against their TM equivalents, in which the TM data acted as independent variable and the MODIS data as dependent variable. The resulting regression slope and intercept equaled respectively 1.31 and -27.97. The MODIS-derived burned area map correlated fairly well with the TM-based map (coefficient of determination  $R^2=0.98$ ,  $p<0.001$ ), although a consistent overestimation relative to the TM data was perceived as indicated by the regression slope of 1.31.

Figure 7A reflects the  $D$  in function of varying number of control pixels and window size for a pre-fire year. It shows the median temporal similarity of the 500 unburned sample pixels. The median is used instead of the mean as it is more robust in the presence of outlier values. Two main effects are observed in the figure. Firstly, the number of control pixels chosen influenced the dissimilarity measure due to an averaging effect. The strength of this averaging effect was dependent on window size: the averaging effect became more important for larger window sizes. Secondly, there was a consistently decreasing trend in pre-fire  $D$  when window

size enlarged. This feature appeared regardless of the number of control pixels chosen. The latter finding contrasts with what is visible in figure 7B, which represents the post-fire  $D$  in function of varying number of control pixels and window size. Here, one can see a consistently increasing trend in  $D$  as window size became larger. As a result, differences between pre- and post-fire similarity enlarged in proportion with window size. This effect originates from the possible selection of distant pixels that have higher probability of showing different post-fire environmental conditions in larger windows (Lhermitte et al. 2010b). Based on figures 7A-B the control pixel selection was calibrated by taking the average of the four most similar pixels out of eight candidate pixels, which corroborates with the findings of Lhermitte et al. (2010b).

#### 4.3 Relationship between field, TM and MODIS data

Table 3 lists some descriptive statistics as derived from the  $\text{dNBR}_{\text{TM,IA}}$ ,  $\text{dNBR}_{\text{TM,EA}}$ ,  $\text{dNBR}_{\text{MODIS,IA}}$  and  $\text{dNBR}_{\text{MODIS,EA}}$  layers. Mean dNBR was clearly higher for an IA than for an EA, for both TM and MODIS assessments (0.56 vs. 0.29 for TM, 0.44 vs. 0.21 for MODIS). The same was true for mean optimality (0.65 vs. 0.47 for TM, 0.68 vs. 0.50 for MODIS). The standard deviation (sd) of the dNBR sd was also higher in IA than in EA (0.29 vs. 0.19 for TM, 0.19 vs. 0.14 for MODIS). This contrasts with the lower optimality sd of IAs compared to EAs (0.25 vs. 0.29 for TM, 0.24 vs 0.30 for MODIS). Mean and sd dNBR were higher for TM assessment than for MODIS assessments. Mean optimality, however, was slightly higher for MODIS assessments, while inter-sensor differences in sd optimality were minor.

Table 4 summarizes the regression results between field, TM and MODIS data. All results were based on 150 observations, corresponding to the GeoCBI locations. Comparison of the  $R^2$  statistics shows that the GeoCBI-dNBR<sub>TM</sub> relationship proved to be the strongest for the IA scheme. This relationship yielded a moderate-high  $R^2 = 0.72$  for a linear fitting model.

This is higher than the GeoCBI-dNBR<sub>TM,EA</sub> correlation which had an  $R^2 = 0.56$ . After downsampling the TM pixels to the MODIS resolution, linear regressions were also performed between the downsampled TM and the MODIS dNBR. These regressions resulted in a moderate correlations of  $R^2 = 0.59$  for the IA and  $R^2 = 0.45$  for the EA scheme.

#### **4.4 Post-fire MODIS dNBR and optimality time series**

##### **4.4.1 Shrub land**

Figure 8A displays the temporal profiles of mean NBR ( $\pm$  sd) of both control and focal pixels. The control pixels' NBR values remained more or less constant around 0.40 ( $\pm$  0.10) throughout the year, except for the early spring peak (April-May), which is characteristic for xerophytic shrub species (see also figure 4A). The fire event caused a sudden drop in the focal pixels' mean NBR values up to -0.18 ( $\pm$  0.14) at the third post-fire composite. This was followed by a relatively quick recovery which culminated in early spring when the burned pixels achieved NBR values of 0.40. During the first half year post-fire the control pixels' sd NBR was relatively high around 0.20. Near the fire's anniversary date the focal pixels' mean NBR values dropped back to values of 0.20, but also the sd dropped to 0.10.

Figure 8B depicts mean dNBR ( $\pm$  sd) against time relative to the fire event. A maximum mean dNBR of 0.48 ( $\pm$  0.18) was reached at the third post-fire composite. These relatively high mean and sd values progressively degraded. During spring-time mean dNBR was only 0.11 ( $\pm$  0.13), after which mean dNBR values slightly recovered up to 0.18 ( $\pm$  0.11) around the fire's anniversary date.

The temporal evolution of mean optimality ( $\pm$  sd) is shown in figure 8C. Mean optimality peaked at the fourth post-fire composite (0.73  $\pm$  0.21), however, mean optimality decreased to 0.23 ( $\pm$  0.28) during spring. Afterwards mean optimality increased back to values around 0.49 ( $\pm$  0.30).

#### 4.4.2 Coniferous forest

In figure 9A one can see the post-fire development of mean NBR ( $\pm$  sd) time series of control and focal pixels. Similar to what was observed in figure 4B, the control pixels' mean reveals little seasonal variation, with values around 0.50 ( $\pm$  0.10) throughout the year. At the third post-fire composite the focal pixels' mean NBR dropped to -0.16 ( $\pm$  0.19). While the focal pixels' mean NBR steadily increased to values around 0.20 at the fire's anniversary date, their sd NBR decreased to 0.11. Likewise the spring-time peak observed for shrub lands, the focal pixels also experience a slight increase in NBR during early spring.

In figure 9B it is observed that the maximum mean dNBR, which was reached at the third post-fire composite equaled 0.61 ( $\pm$  0.22). Both mean and sd then gradually decreased to values around respectively 0.30 and 0.14 at the fire's anniversary date.

Figure 9C displays the temporal profile of mean optimality ( $\pm$  sd) during the one-year post-fire period. Mean optimality reached a maximum of 0.71 ( $\pm$  0.21) at the fourth post-fire composite. Mean optimality was almost continuously between 0.50 and 0.70, except during April-May when it dropped to values of 0.40.

#### 4.4.3 Olive groves

The same as in figure 4C, the mean NBR of the control pixels realized slightly higher values during the wet winter than in the dry summer (figure 10A). The focal pixels' temporal development, however, showed a markedly similar pattern as what was observed for shrub lands in figure 8A. Initially NBR drops, e.g. at the third post-fire composite mean NBR of control pixels' equaled 0.34 ( $\pm$  0.08), compared to a focal pixels' mean of -0.12 ( $\pm$  0.13). Then the burned pixels' NBR values peaked during April-May resulting in mean NBR values of 0.40 ( $\pm$  0.08). Finally, the focal pixels' mean NBR decreased back to values of 0.21 ( $\pm$  0.10) during the one-year post-fire summer.

Figure 10B depicts the mean dNBR ( $\pm$  sd) against time. After reaching a maximum mean dNBR of 0.46 ( $\pm$  0.16) at the third post-fire composite, a minimum mean dNBR of 0.10 ( $\pm$  0.11) was reached during spring-time. After obtaining this minimum, the mean dNBR recovered to values of 0.19 ( $\pm$  0.11). Overall this temporal pattern in mean dNBR shows a high similarity to what is described in section 4.4.1 for shrub lands.

The mean optimality's maximum occurred at the fourth post-fire composite and equaled 0.73 ( $\pm$  0.23) (figure 10C). During winter and spring, optimality dropped to values around 0.30 ( $\pm$  0.30). In the first post-fire summer, however, mean optimality again reached values around 0.55 ( $\pm$  0.28).

#### **4.4.4 Deciduous forest**

The mean NBR time series of control pixels showed a marked seasonality with a winter minimum and summer maximum (figure 11A), which corresponds with the findings of figure 4D. Immediately post-fire the difference between the control and focal pixels' mean NBR values is large, e.g. at the third post-fire composite they are respectively 0.47 ( $\pm$  0.06) and -0.15 ( $\pm$  0.18). However, this difference diminished as time elapsed due to two main processes. Firstly, leaf-fall caused the control pixels' index to drop. Secondly, regeneration processes produced an increase of the focal pixels' NBR values. By the start of the next growing season, however, the difference between control and focal pixels became again more explicit.

The above-mentioned processes also provoked a clear seasonality in both temporal mean dNBR (figure 11B) and optimality (figure 11C). Initially mean dNBR values are high with corresponding high optimality scores. At the fourth post-fire composite mean dNBR and optimality were respectively 0.61 ( $\pm$  0.17) and 0.71 ( $\pm$  0.16). During winter dNBR values are very low, a minimum of 0.10 ( $\pm$  0.13) was reached, and this also resulted in low mean

optimality scores below 0.40. By the onset of next growing season both mean dNBR and optimality recovered.

## **5 Discussion**

### **5.1 Lag timing**

Regression results between dNBR<sub>TM</sub> and field data were clearly influenced by the lag timing of the assessment (Table 4). Although this corroborates with the findings of Zhu et al. (2006) and Allen and Sorbel (2008), it contrasts with Fernandez-Manso et al. (2009) who state that the difference between an IA and EA does not significantly influences the remotely sensed magnitude of change. In our study the correlation between field and TM data was better for the IA ( $R^2 = 0.72$ ) than for the EA ( $R^2 = 0.56$ ), which is opposite to the observations of Zhu et al. (2006). Following these authors, however, the poorer regression fits for IA are merely attributed to unfavorable remote sensing conditions (low sun angles, smoke, bad weather, snow and clouds), and not necessarily to differences in lag timing. Additionally, Allen and Sorbel (2008) found that initial and extended assessments produced significantly different information with regards to burn severity for tundra vegetation, while the timing of the assessment had no effect for black spruce forest, which was attributed to the rapid tundra recovery. As in our study, this demonstrates that in quickly recovering ecosystems first-order effects such as vegetation consumption, scorching and charring are mitigated by resprouters (Key, 2006; Lhermitte et al., 2010a). This is also visible when the magnitude of change and the within-burn variation between IA and EA schemes are compared (Table 3). For both TM and MODIS assessment, mean dNBR almost halved whereas sd dNBR was also clearly lower for the EA. This reduction in variability highly impacts the suitability of the dNBR for burn severity mapping. The within-burn variation of the MODIS assessments was lower than with TM assessment as a result of the 500 m resolution compared to the 30 m resolution of the TM



sensor. Correlations between downsampled  $\text{dNBR}_{\text{TM}}$  and corresponding  $\text{dNBR}_{\text{MODIS}}$  were moderate, which justifies the use of MODIS NBR time series as a way of exploring the temporal dimension of remote sensing of post-fire effects. We are aware that by doing so spatial heterogeneity is sacrificed to some degree (Key 2006). Differences between downsampled  $\text{dNBR}_{\text{TM}}$  and  $\text{dNBR}_{\text{MODIS}}$  can be attributed to the use of single-data imagery vs. 8-day composites, discrepancies between traditional bi-temporal differencing and control pixel selection procedure, differences in preprocessing (e.g. modified c-correction vs. no topographic correction), MODIS's geolocation error (Wolfe et al., 1998), etc.

Previous studies have analyzed the  $\text{dNBR}$ 's optimality for assessing fire/burn severity, most of them based on Landsat imagery (Roy et al., 2006; Escuin et al., 2008; Murphy et al., 2008; Veraverbeke et al., 2010bc). This resulted in a moderate mean optimality of 0.49 (Escuin et al., 2008) and between 0.26-0.80 for six burns in Alaska, United States (Murphy et al., 2008). Clearly lower mean  $\text{dNBR}$  optimality scores (0.10) were reported by Roy et al. (2006) for African savannah burns. These authors also report low  $\text{dNBR}$  optimality values for MODIS sensed fires in other ecosystems (Russia, Australia, South America). These results suggest that the  $\text{dNBR}$  is suboptimal for assessing fire/burn severity. The poor optimality results obtained by Roy et al. (2006) can partly be explained by the fact that the authors also included unburned pixels in their analysis. Unaffected pixels are generally associated with low optimality scores since a pixel's shift in the bi-spectral space is then only caused by noise (Escuin et al., 2008). Veraverbeke et al. (2010c) revealed the influence of illumination effects on  $\text{dNBR}$  optimality after which they proposed a topographic correction that significantly improved the reliability of the assessment. Despite of the merits of these studies, none of them researched the time-dependency of the optimality statistic. The descriptive optimality statistics (Table 3) reveal the influence of assessment timing on the performance of the  $\text{dNBR}$ . The IAs had clearly higher optimality scores than EAs, e.g. for the TM assessment

respectively 0.65 ( $\pm$  0.25) and 0.47 ( $\pm$  0.29). Mean optimality values achieved a maximum at the third or fourth post-fire composite (Figures 8C, 9C, 10C and 11C). At the moment of maximum optimality, the sd of the optimality statistic reached its minimum elucidating its stability. Based on the optimality statistic one can indicate three to four weeks post-fire as the best moment to assess post-fire effects, at least in this study. This moment also corresponds with the highest magnitude of change in dNBR (figures 8B, 9C, 10C and 11C) and with a relatively high degree in variation. Results based on our TM data slightly differ from previously published outcomes based on the same data (Veraverbeke 2010abc), mainly because of some minor changes in satellite preprocessing and the exclusion of 10 unburned field plots.

## **5.2 Seasonal timing**

An important recommendation when doing bi-temporal change detection is that the image couple should approximate as closely as possible the anniversary date acquisition scheme (Coppin et al., 2004). This diminishes illumination differences and phenological dissimilarities. Because of Landsat's infrequent acquisition of cloud-free imagery (Ju and Roy, 2008) bi-temporal acquisition schemes potentially diverge from the ideal anniversary data scheme. This causes problems as external influences (e.g. illumination conditions, plant phenology) then distort the evaluation of post-fire effects (Verbyla et al., 2008; Veraverbeke et al., 2010c). Verbyla et al. (2008) demonstrated false trends in dNBR as a consequence of combined seasonal and topographic effects, while Veraverbeke et al. (2010c) recommended performing topographic corrections, even for ratio-based analysis, as the general assumption that ratioing reflectance data removes shade effects does not necessarily hold true. These issues are merely concerned with traditional image-to-image normalization constraints (Song and Woodcock, 2003). The application of the control pixel selection procedure, however, makes the MODIS dNBR time series free of these limitations (Diaz-Delgado and Pons, 2001;

Lhermitte et al., 2010b). Comparison of figures 8-11 discloses some important findings. Firstly, only slight differences in assessment timing can result in distinct index values. On the one side this results from recovery processes (see section 5.1), but on the other side seasonal changes in both control and focal pixels are also important. In our study area for example, the herbaceous resprouters show a clear rise in NBR values during spring, which is a period of favorable hydro-thermic conditions (figure 3, Specht, 1981; Maselli, 2004). As a consequence corresponding dNBR and optimality values dramatically drop during this period. In the one-year post-fire summer productivity of regenerating plants diminishes again which results in a generally better index performance. Secondly, phenological patterns can greatly vary between different land cover types (Reed et al., 1994; Viovy, 2000, Lhermitte et al., 2008). Figure 11A, which displays the NBR time series of deciduous forest, contrasts with those of figures 8A, 9A and 10A. This is because the evergreen land cover types (shrub land, coniferous forest and olive groves) typically have a productivity that remains more or less stable throughout the year while deciduous forest is characterized by a clear winter minimum and summer maximum. As a consequence, while the seasonal timing of an assessment produces only small differences for evergreen species, it is crucial for deciduous forest. When this consideration is forgotten, an assessment in deciduous land cover types risks to measure plant phenology (e.g. leaf senescence) instead of the fire effects, which can falsify fire/burn severity estimations. Similar findings were achieved by Lhermitte et al. (2010a). In this study, conducted in a savanna environment, intra-annual changes in index values were dominated by the grass layer. The assessment was therefore strongly influenced by its seasonal timing. Summarized for our study area, a Mediterranean-type ecosystem (MTE) with a mixture of land covers, the summer period is preferential for fire/burn severity assessments. This timing reduces the occurrence of phenological discrepancies between different land covers.

### **5.3 Implications for Landsat dNBR fire/burn severity assessments**

645 Increasingly, fire researchers become interested in detecting trends in fire/burn severity  
646 (Eidenshink et al., 2007; Miller et al., 2008; Verbyla et al., 2008). To fulfill this duty it is of  
647 paramount importance that assessment are comparable across space and time. The relative  
648 version of the dNBR (RdNBR), which is defined as the dNBR divided by the square root of  
649 the pre-fire NBR, hypothetically allows a better comparison among different land cover types,  
650 especially in heterogeneous landscapes. This was made clear for fires in conifer dominated  
651 vegetation types in California, USA (Miller et al., 2009). Whether the hypothetical advantage  
652 of the relative index to account for spatial heterogeneity has an intuitive appeal, the index  
653 does not handle temporal differences which may be present among different assessments. In  
654 this respect our study demonstrates that only small differences in Landsat acquisition timing  
655 can result in significantly other dNBR and optimality values. This results from both lag and  
656 seasonal constraints. The latter requires a profound knowledge of the covers affected by the  
657 fire and their phenological development, especially when the land covers reveal dissimilar  
658 intra-annual patterns. Lag timing is important as vegetation regrowth mitigates first-order fire  
659 effects (Key et al., 2006; Zhu et al., 2006). This affects the magnitude of change, the  
660 variability and the index performance of what is actually measured. For our Mediterranean  
661 study area, correlation with field data, dNBR variability and optimality were clearly higher  
662 for an IA than for an EA. Additionally, optimality was the highest three to four weeks post-  
663 fire, and not immediately post-fire. In other ecosystems, however, EAs trended better with  
664 field data (Zhu et al., 2006). The NBR was originally developed for the use in temperate and  
665 boreal ecosystems (Key and Benson, 2005; Eidenshink et al., 2007; French et al., 2008 among  
666 them), which are characterized by a relative slow recovery (Cuevas-Gonzalez et al., 2009).  
667 For these ecoregions it is plausible that lag timing not significantly alters the information  
668 content of an assessment. The lag timing of assessment in quickly recovering ecosystems,  
669 however, determines how post-fire effects are measured. Fire severity is estimated with better

contrast and higher reliability, while first-order effects are obscured by regeneration processes when assessing burn severity. This incites caution for the use of the NBR for assessing burn severity in quickly recovering ecosystems.

Of course bi-temporal Landsat assessments are limited by the infrequent image availability (Ju and Roy, 2009). Moreover, whether or not ecosystem responses are included in the study makes an important ecological difference and depends on the goals of the project. Within these limitations, however, one should be aware of the temporal dimension of the remote sensing of post-fire effects. In this context, we urge for a transparent and consistent use of terminology as presented in figure 1. In this we follow Lentile et al. (2006) who suggested a substantial difference between the terms fire and burn severity. From a remote sensing point of view, our results support this important difference and question the recommendation of Keeley (2009) to treat both terms as mutually interchangeable. Both terms assess the direct fire impact but only burn severity includes ecosystem responses.

## **6 Conclusions**

The goal of this paper was to elaborate on the temporal dimension of dNBR fire/burn severity studies. In this context fire severity was defined as the degree of environmental change caused by fire as measured immediately post-fire, whereas burn severity combines the direct fire impact and ecosystem responses. The study made use of field, TM and MODIS data. An IA and EA were calculated based on pre-/post-fire differenced TM imagery. Additionally a MODIS dNBR time series was generated by using the control pixel selection procedure. This procedure uses the time series similarity concept to assign a unique control pixel to each burned pixel, which allows differencing within the same image. The large 2007 Peloponnese (Greece) wildfires were chosen as case study.

Results showed a clearly better correlation with field data for the IA than for the EA. In addition, the magnitude, variability and optimality of the dNBR were better early post-fire than one-year post-fire. Moreover, the highest index optimality was reached three to four weeks post-fire. In quickly recovering ecosystems, thus, regeneration processes mitigate first-order fire effects, which can obscure burn severity estimations. This demonstrates the influence of the lag timing of an assessment. Results also revealed that land cover specific intra-annual variations influence to a high degree dNBR and optimality outcomes. For example in the Mediterranean, favorable hydro-thermic conditions during spring enhance the productivity of herbaceous species in the burned areas. This, however, makes the dNBR unsuitable to measure fire-effects during this period. As such, an appropriate seasonal timing of an assessment is of paramount importance to minimize false trends. Although these findings are specific to our case study, similar temporal constraints can be expected in other ecoregions. Our findings urge, within the limitations of available Landsat imagery, for awareness of the temporal dimension in the remote sensing of post-fire effects. In this context, we also propose clarification in associated terminology.

## **Acknowledgements**

The study was financed by the Ghent University special research funds (BOF: Bijzonder Onderzoeksfonds). The authors would like to thank the anonymous reviewers for their constructive remarks.

## **References**

Allen, J., & Sorbel, B., 2008. Assessing the differenced Normalized Burn Ratio's ability to map burn severity in the boreal forest and tundra ecosystems of Alaska's national parks *International Journal of Wildland Fire*, 17, 463-475

716 Barbosa, M., Pereira, J. & Gregoire, J. (1998). Compositing criteria for burned area  
717 assessment using multitemporal low resolution satellite data. *Remote Sensing of Environment*,  
718 65, 38-49

719 Barbosa, P., Gregoire, J., & Pereira, J. (1999). An algorithm for extracting burned areas from  
720 time series of AVHRR GAC data applied at a continental scale. *Remote Sensing of*  
721 *Environment*, 69, 253-263

722 Bisson, M., Fornaciai, A., Coli, A., Mazzarini, F. & Pareschi, M. (2008). The Vegetation  
723 Resilience After Fire (VRAF) index: Development, implementation and an illustration from  
724 central Italy, *International Journal of Applied Earth Observation and Geoinformation*, 10,  
725 312-329

726 Brewer, K., Winne, C., Redmond, R., Opitz, D. & Mangrich, M. (2005). Classifying and  
727 mapping wildfire severity: a comparison of methods. *Photogrammetric Engineering &*  
728 *Remote Sensing*, 71, 1311-1320

729 Capitaino, R., & Carcaillet, C. (2008). Post-fire Mediterranean vegetation dynamics and  
730 diversity: a discussion of succession models. *Forest Ecology and Management*, 255, 431–439

731 Chafer, C., Noonan, M. & Macnaught, E. (2004). The post-fire measurement of fire severity  
732 and intensity in the Christmas 2001 Sydney wildfires. *International Journal of Wildland Fire*,  
733 13, 227-240

734 Chafer, C. (2008). A comparison of fire severity measures: an Australian example and  
735 implications for predicting major areas of soil erosion. *Catena*, 74, 235–245

736 Chander G., Markham, L. & Barsi, J. (2007). Revised Landsat-5 Thematic Mapper  
737 radiometric calibration. *IEEE Geoscience and Remote Sensing Letters*, 4, 490–494

738 Chavez, P. (1996). Image-based atmospheric corrections – revisited and improved.  
739 *Photogrammetric Engineering & Remote Sensing*, 6, 1025–1036

740 Chuvieco, E., Ventura, G., Martin, P. & Gomez, I. (2005). Assessment of multitemporal  
 741 compositing techniques of MODIS and AVHRR images for burned land mapping. *Remote*  
 742 *Sensing of Environment*, 94, 450-462

743 Chuvieco, E., Englefield, P., Trishchenko, A. & Luo, Y. (2008). Generation of long time  
 744 series of burn area maps of the boreal forest from NOAA-AVHRR composite data. *Remote*  
 745 *Sensing of Environment*, 112, 2381-2396

746 Cihlar, J. (1996). Identification of contaminated pixels in AVHRR composite images for  
 747 studies of land biosphere. *Remote Sensing of Environment*, 56, 149-163

748 Cocke, A., Fule, P. & Crouse, J. (2005). Comparison of burn severity assessments using  
 749 Differenced Normalized Burn Ratio and ground data. *International Journal of Wildland Fire*,  
 750 14, 189-198

751 Coppin, P., Jonckheere, I., Nackaerts, K., & Muys, B., (2004). Digital change detection  
 752 techniques in ecosystem monitoring: a review. *International Journal of Remote Sensing*, 25,  
 753 1565-1595

754 Cuevas-Gonzalez, M., Gerard, F., Baltzer, H., & Riano, D. (2009). Analysing forest recovery  
 755 after wildfire disturbance in boreal Siberia using remotely sensed vegetation indices. *Global*  
 756 *Change Biology*, 15, 561-577

757 De Santis, A. & Chuvieco, E. (2009). GeoCBI: a modified version of the Composite Burn  
 758 Index for the initial assessment of the short-term burn severity from remotely sensed data.  
 759 *Remote Sensing of Environment*, 113, 554-562

760 Diaz-Delgado, R. & Pons, X. (2001). Spatial patterns of forest fires in Catalonia (NE of  
 761 Spain) along the period 1975-1995: analysis of vegetation recovery after fire. *Forest Ecology*  
 762 *and Management*, 147, 67-74



763 Diaz-Delgado, R., Lloret, F., & Pons, X. (2003). Influence of fire severity on plant  
764 regeneration by means of remote sensing. *International Journal of Remote Sensing*, 24, 1751-  
765 1763

766 Dwyer, E., Perreira, J., Grégoire, J. & DaCamara, C. (1999). Characterization of the spatio-  
767 temporal patterns of global fire activity using satellite imagery for the period April 1992 to  
768 March 1993. *Journal of Biogeography*, 27, 57-69

769 Eidenshink, J., Schwind, B., Brewer, K., Zhu, Z., Quayle, B. & Howard, S. (2007). A project  
770 for monitoring trends in burn severity. *Fire Ecology*, 3, 3-21

771 Epting, J., & Verbyla, D. (2005). Landscape-level interactions of prefire vegetation, burn  
772 severity, and postfire vegetation over a 16-year period in interior Alaska. *Canadian Journal*  
773 *Forest Research*, 35, 1367-1377

774 Epting, J., Verbyla, D. & Sorbel, B. (2005). Evaluation of remotely sensed indices for  
775 assessing burn severity in interior Alaska using Landsat TM and ETM+. *Remote Sensing of*  
776 *Environment*, 96, 328-339

777 Escuin, S., Navarro, R. & Fernandez, P. (2008). Fire severity assessment by using NBR  
778 (Normalized Burn Ratio) and NDVI (Normalized Difference Vegetation Index) derived from  
779 LANDSAT TM/ETM images, *International Journal of Remote Sensing*, 29, 1053-1073

780 Fernandez-Manso, O., Quintano, C., & Fernandez-Manso, A. (2009). Combining spectral  
781 mixture analysis and object-based classification for fire severity mapping. *Investigacion*  
782 *Agraria: Sistemas y Recursos Forestales*, 18, 296-313

783 Fox, D., Maselli, F., & Carrega, P. (2008). Using SPOT images and field sampling to map  
784 burn severity and vegetation factors affecting post forest fire erosion risk. *Catena*, 75, 326-  
785 335

786 French, N., Kasischke, E., Hall, R., Murphy, K., Verbyla, D., Hoy, E. & Allen, J. (2008).  
787 Using Landsat data to assess fire and burn severity in the North American boreal forest  
788 region: an overview and summary of results. *International Journal of Wildland Fire*, 17, 443-  
789 462

790 Garmin, (2005) Garmin eTrex Vista personal navigator. Owner's manual and reference guide.  
791 Available from: [https://buy.garmin.com/shop/store/manual.jsp?product=010-00243-](https://buy.garmin.com/shop/store/manual.jsp?product=010-00243-00&cID=167&pID=163)  
792 [00&cID=167&pID=163](https://buy.garmin.com/shop/store/manual.jsp?product=010-00243-00&cID=167&pID=163) (Last visited on 24/02/2010).

793 Geerken, R., Zaitchik, B. & Evans, J. (2005). Classifying rangeland vegetation type and  
794 fractional cover of semi-arid and arid vegetation cover from NDVI time-series. *International*  
795 *Journal of Remote Sensing*, 24, 5535-5554

796 Gonzalez-Alonso, F., Merino-De-Miguel, S., Roldan-Zamarron, A., Garcia-Gigorro, S. &  
797 Cuevas, J. (2007). MERIS Full Resolution data for mapping level-of-damage caused by forest  
798 fires: the Valencia de Alcántara event in August 2003. *International Journal of Remote*  
799 *Sensing*, 28, 789-809

800 Hammill, K., & Bradstock, R. (2006). Remote sensing of fire severity in the Blue Mountains:  
801 influence of vegetation type and inferring fire intensity. *International Journal of Wildland*  
802 *Fire*, 15, 213-226

803 Holben, B. (1986). Characteristics of maximum-value composite images from temporal  
804 AVHRR data. *International Journal of Remote Sensing*, 7, 1417-1434

805 Hudak, A., Morgan, P., Bobbitt, M., Smith, A., Lewis, S., Lentile, L., Robichaud, P., Clark,  
806 J., & McKinley, R. (2007). The relationship of multispectral satellite imagery to immediate  
807 fire effects. *Fire Ecology*, 3, 64–90

808 Isaev, A., Korovin, G., Bartalev, S., Ershov, D., Janetos, A., Kasischke, E., Shugart, H.,  
809 French, N, Orlick, B. & Murphy, T. (2002). Using remote sensing to assess Russian forest fire  
810 carbon emissions. *Climatic Change*, 55, 239-245

811 Jain, T., Pilliod, D. & Graham, R. (2004). Tongue-tied. *Wildfire*, 4, 22–26

812 Jarvis, A., Reuter, H., Nelson, A., Guevara, E. (2006). Hole-filled seamless SRTM data V3.  
813 Available from: <http://srtm.csi.cgiar.org> (Last visited on 24/02/2010)

814 Jonsson, P. & Eklundh, L. (2004). TIMESAT-a program for analyzing time-series of satellite  
815 sensor data. *Computers & Geosciences*, 30, 833-845

816 Ju, J., & Roy, D. (2008). The availability of cloud-free Landsat ETM+ data over the  
817 conterminous United States and globally. *Remote Sensing of Environment*, 112, 1196-1211

818 Kasischke, E. & French, N. (1995). Locating and estimating the areal extent of wildfires in  
819 Alaskan boreal forests using multiple-season AVHRR NDVI composite data. *Remote Sensing*  
820 *Environment*, 51, 263-275

821 Keeley, J. (2009). Fire intensity, fire severity and burn severity: a brief review and suggested  
822 usage. *International Journal of Wildland Fire*, 18, 116-126

823 Key, C. & Benson, N. (2005). Landscape assessment: ground measure of severity; the  
824 Composite Burn Index, and remote sensing of severity, the Normalized Burn Index. In D.  
825 Lutes, R. Keane, J. Caratti, C. Key, N. Benson, S. Sutherland & L. Gangi (Eds.), *FIREMON:*  
826 *Fire effects monitoring and inventory system* (pp. 1-51). USDA Forest Service, Rocky  
827 Mountains Research Station, General Technical Report RMRS-GTR-164-CD LA

828 Key, C., (2006). Ecological and sampling constraints on defining landscape fire severity. *Fire*  
829 *Ecology*, 2, 34–59

830 Kutiel, P., & Inbar, M. (1993). Fire impacts on soil nutrients and soil erosion in a  
831 Mediterranean pine forest plantation. *Catena*, 20, 129–139

832 Landmann, T. (2003). Characterizing sub-pixel Landsat ETM+ fire severity on experimental  
833 fire in the Kruger National Park, South Africa. *South African Journal of Science*, 99, 357-359

834 Lee, B., Kim, S., Chung, J. & Park, P., (2008). Estimation of fire severity by use of Landsat  
835 TM images and its relevance to vegetation and topography in the 2000 Samcheok forest fire.  
836 *Journal of Forest Research*, 13, 197-204

837 Lentile, L., Smith, F. & Shepperd, W. (2005). Patch structure, fire-scar formation, and tree  
838 regeneration in a large mixed-severity fire in the South Dakota Black Hills, USA. *Canadian*  
839 *Journal Forest Research*, 35, 2875-2885

840 Lentile, L., Holden, Z., Smith, A., Falkowski, M., Hudak, A., Morgan, P., Lewis, S., Gessler,  
841 P., & Benson, N. (2006). Remote sensing techniques to assess active fire characteristics and  
842 post-fire effects. *International Journal of Wildland Fire*, 15, 319-345

843 Lhermitte, S., Verbesselt, J., Jonckheere, I., Nackaerts, K., van Aardt, J., Verstraeten, W.W.,  
844 & Coppin, P. (2008). Hierarchical image segmentation based on similarity of NDVI time  
845 series. *Remote Sensing of Environment*, 112, 506-521

846 Lhermitte, S., Verbesselt, J., Verstraeten, W.W., Veraverbeke, S., & Coppin, P. (2010a).  
847 Assessing intra-annual vegetation regrowth after fire using the pixel based regeneration index.  
848 *ISPRS Journal of Photogrammetry and Remote Sensing*, submitted for publication.

849 Lhermitte, S., Verbesselt, J., Verstraeten, W.W., & Coppin, P. (2010b). A pixel based  
850 regeneration index using time series similarity and spatial context. *Photogrammetric*  
851 *Engineering and Remote Sensing*, accepted for publication

852 Lopez-Garcia, M. & Caselles, V. (1991). Mapping burns and natural reforestation using  
853 Thematic Mapper data. *Geocarto International*, 6, 31-37

854 Maselli, F. (2004). Monitoring forest conditions in a protected Mediterranean coastal area by  
855 the analysis of multiyear NDVI data. *Remote Sensing of Environment*, 89, 423-433

856 Miller, J., & Thode, A., (2007). Quantifying burn severity in a heterogenous landscape with a  
857 relative version of the delta Normalized Burn Ratio (dNBR). *Remote Sensing of Environment*,  
858 109, 66–80

859 Miller, J., Safford, H., Crimmins, M., & Thode, A., (2008). Quantitative evidence of  
860 increasing forest fire severity in the Sierra Nevada and southern Cascade mountains,  
861 California and Nevada, US. *Ecosystems*, 12, 16-32

862 Miller, J., Knapp, E., Key, C., Skinner, C., Isbell, C., Creasy, R., Sherlock, J. (2009).  
863 Calibration and validation of the relative differenced Normalized Burn Ratio (RdNBR) to  
864 three measures of fire severity in the Sierra Nevada and Klamath Mountains, California, USA.  
865 *Remote Sensing of Environment*, 113, 645–656

866 Murphy, K., Reynolds, J. & Koltun, J. (2008). Evaluating the ability of the differenced  
867 Normalized Burn Ratio (dNBR) to predict ecologically significant burn severity in Alaskan  
868 boreal forests. *International Journal of Wildland Fire*, 17, 490-499

869 Olsson, L. & Eklundh, L. (1994). Fourier-series for analysis of temporal sequences of satellite  
870 sensor imagery. *International Journal of Remote Sensing*, 15, 3735-3741

871 Pausas, J. (2004). Changes in fire and climate in the eastern Iberian peninsula (Mediterranean  
872 Basin). *Climatic Change*, 63, 337-350

873 Pereira, J., Sa, A., Sousa, A., Silva, J., Santos, T. & Carreiras, J. (1999). Spectral  
874 characterization and discrimination of burnt areas. In Chuvieco, E. (Ed.), *Remote sensing of*  
875 *large wildfires in the European Mediterranean Basin* (pp. 123-138). Berlin: Springer-Verlag

876 Perez-Cabello, F., de la Riva Fernandez, J., Montorio Lloveria, R. & Garcia-Martin, A.  
877 (2006). Mapping erosion-sensitive areas after wildfires using fieldwork, remote sensing, and  
878 geographic information systems techniques on a regional scale. *Journal of Geophysical*  
879 *Research*, 111, G04S10

880 Reed, B., Brown, J., Vanderzee, D., Loveland, T., Merchant, J. & Ohlen, D. (1994).  
881 Measuring phenological variability from satellite imagery. *Journal of Vegetation Science*, 15,  
882 703-714

883 Riano, D., Moreno-Ruiz, J., Isidoros, D. & Ustin, S. (2007). Global spatial patterns and  
884 temporal trends of burned area between 1981 and 2000 using NOAA-NASA Pathfinder.  
885 *Global Change Biology*, 13, 40-50

886 Roder, A., Hill, J., Duguy, B., Alloza, J. & Vallejo, R. (2008). Using long time series of  
887 Landsat data to monitor fire events and post-fire dynamics and identify driving factors. A case  
888 study in the Ayora region (eastern Spain). *Remote Sensing of Environment*, 112, 259-273

889 Roy, D., Boschetti, L. & Trigg, S. 2006. Remote sensing of fire severity: assessing the  
890 performance of the Normalized Burn Ratio. *IEEE Transactions on Geoscience and Remote*  
891 *Sensing*, 3, 112-116

892 Ruiz-Gallardo, J., Castano, S. & Calera, A. 2004. Application of remote sensing and GIS to  
893 locate priority intervention areas after wildland fires in Mediterranean systems: a case study  
894 from south-eastern Spain. *International Journal of Wildland Fire*, 13, 241-252

895 Savitzky, A. & Golay, M. (1964). Smoothing and differentiation of data by simplified least  
896 squares procedures. *Analytical Chemistry*, 36, 1627-1639

897 Specht, R. (1981). Primary production in Mediterranean-climate ecosystems regenerating  
898 after fire. In F. di Castri, D. Goodall, & R. Specht (Eds.), *Mediterranean-type shrublands*.  
899 (pp. 257-267). Amsterdam: Elsevier

900 Song, C., & Woodcock, C. (2003). Monitoring forest succession with multitemporal Landsat  
901 images: factors of uncertainty. *IEEE Transactions on Geoscience and Remote Sensing*, 41,  
902 2557-2567

903 Stow, D., Petersen, A., Rogan, J. & Franklin, J. (2007). Mapping burn severity of  
904 Mediterranean-type vegetation using satellite multispectral data. *GIScience & Remote*  
905 *Sensing*, 44, 1-23

906 Stroppiana, D., Pinnock, S., Pereira, J., & Gregoire, J. (2002). Radiometric analysis of SPOT-  
907 VEGETATION images for burnt area detection in Northern Australia. *Remote Sensing of*  
908 *Environment*, 82, 21-37

909 Teillet, P., Guindon, B. & Goodenough, D. (1982). On the slope-aspect correction of  
910 multispectral scanner data. *Canadian Journal of Remote Sensing*, 8, 84–106

911 Thomas, J., Walsh, R., & Shakesby, R. (1999). Nutrient losses in eroded sediment after fire in  
912 eucalyptus and pine forests in the wet Mediterranean environment of northern Portugal.  
913 *Catena*, 36, 283-302

914 Trabaud, L. (1981). Man and fire: impacts on Mediterranean vegetation. In F. di Castri, D.  
915 Goodall, & R. Specht (Eds.), *Mediterranean-type shrublands*. (pp. 523-537). Amsterdam:  
916 Elsevier

917 Veraverbeke, S., Lhermitte, S., Verstraeten, W.W., & Goossens, R. (2010a). Evaluation of  
918 pre/post-fire differenced spectral indices for assessing burn severity in a Mediterranean  
919 environment with Landsat Thematic Mapper. *International Journal of Remote Sensing*,  
920 accepted for publication

921 Veraverbeke, S., Verstraeten, W., Lhermitte, S., & Goossens, R., (2010b). Evaluation Landsat  
 922 Thematic Mapper spectral indices for estimating burn severity of the 2007 Peloponnese  
 923 wildfires in Greece. *International Journal of Wildland Fire*, accepted for publication

924 Veraverbeke, S., Verstraeten, W.W., Lhermitte, S., & Goossens, R. (2010c). Illumination  
 925 effects on the differenced Normalized Burn Ratio's optimality for assessing fire severity.  
 926 *International Journal of Applied Earth Observation and Geoinformation*, 12, 60-70

927 Verbyla, D., Kasischke, E., & Hoy, E. (2008). Seasonal and topographic effects on estimating  
 928 fire severity from Landsat TM/ETM+ data. *International Journal of Wildland Fire*, 17, 527-  
 929 534

930 Verbesselt, J., Jonsson, P., Lhermitte, S., Jonckheere, I., van Aardt, J. & Coppin, P. (2006).  
 931 Relating time-series of meteorological and remote sensing indices to monitor vegetation  
 932 moisture dynamics. In Chen, C. (Ed.), *Signal and image processing for remote sensing* (pp.  
 933 153-173). Darmouth: CRC press

934 Vermote, E., El Saleous, N. & Justice, C. (2002). Atmospheric correction of MODIS data in  
 935 the visible to middle infrared: first results. *Remote Sensing of Environment*, 83, 97-111

936 Verstraete, M. & Pinty, B. (1996). Designing optimal spectral indexes for remote sensing  
 937 applications. *IEEE Transactions on Geoscience and Remote Sensing*, 34, 1254-1265

938 Viedma, O., Melia, J., Segarra, D. & Garcia-Haro, J. (1997). Modeling rates of ecosystem  
 939 recovery after fires by using Landsat TM data. *Remote Sensing of Environment*, 61, 383-398

940 Viovy, N. (2000). Automatic classification of time series (ACTS): a new clustering method  
 941 for remote sensing time series. *International Journal of Remote Sensing*, 21, 1537-1560

942 White, J., Ryan, K., Key, C., & Running, S. (1996). Remote sensing of forest fire severity and  
 943 vegetation recovery. *International Journal of Wildland Fire*, 6, 125-136



Wolfe, R., Roy, D., & Vermote, E. (1998). MODIS land data storage, gridding, and compositing methodology: level 2 grid. *IEEE Transactions on Geosciences and Remote Sensing*, 36, 1324-1338

Zhu, Z., Key, C., Ohlen, D., & Benson, N., (2006). Evaluate sensitivities of burn-severity mapping algorithms for different ecosystems and fire histories in the United States. Final Report to the Joint Fire Science Program: Project JFSP 01-1-4-12, US Department of Interior (Sioux Falls, SD), pp. 1-36

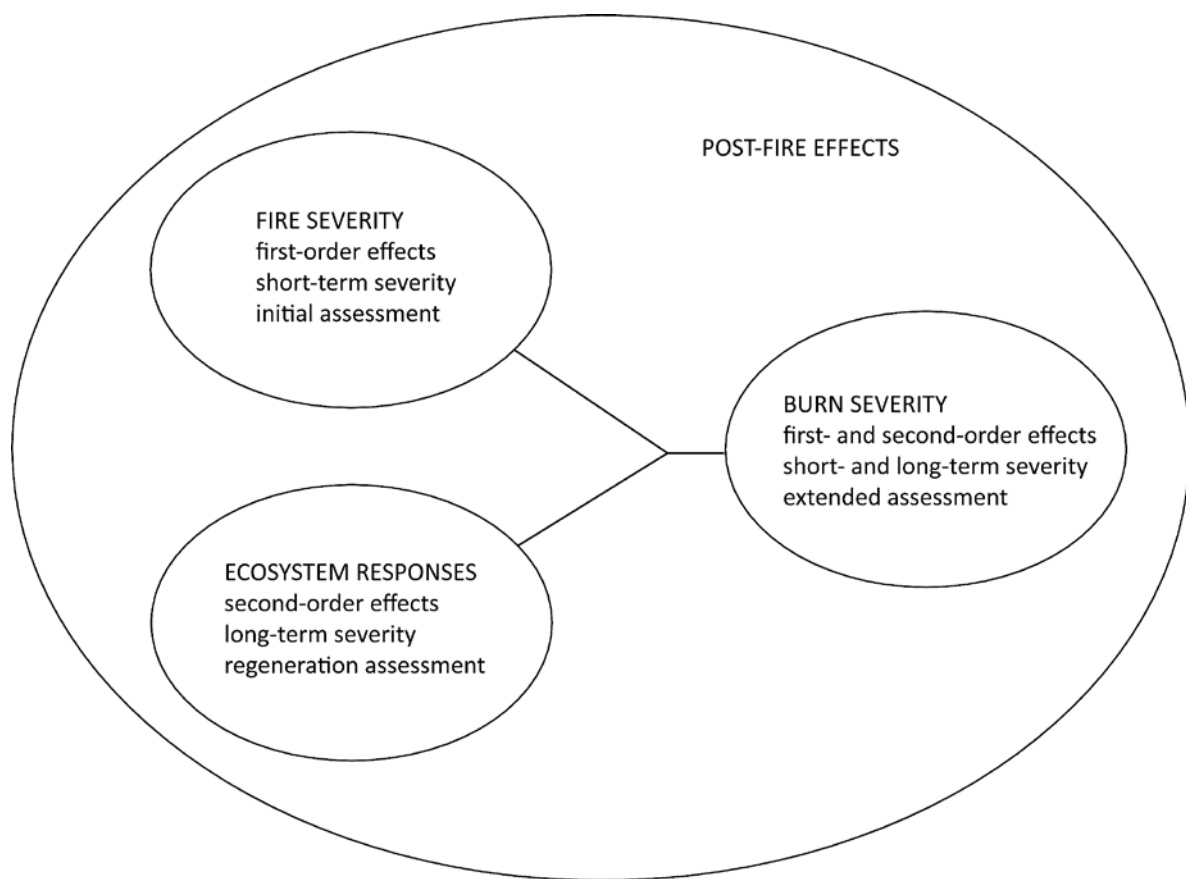
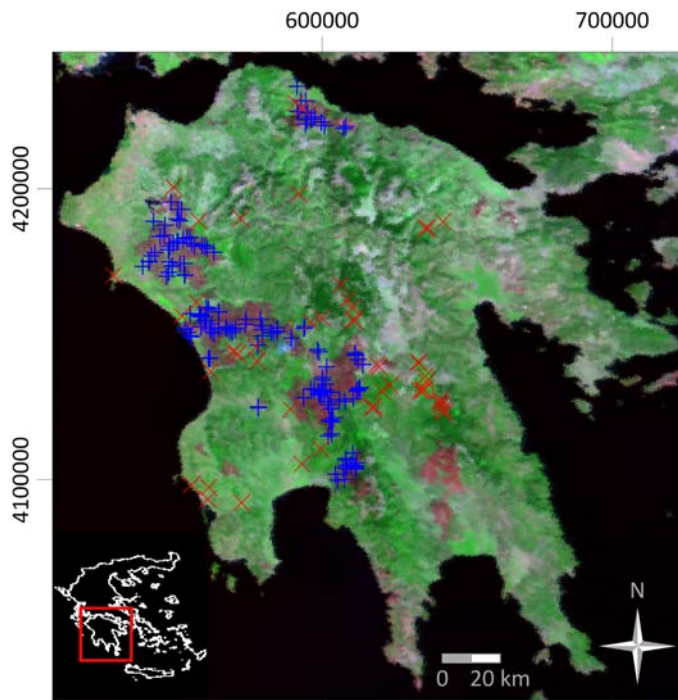


Figure 1. Schematic representation of post-fire effects terminology.

961



962

963 Figure 2. Location of the study area (MODIS daily surface reflectance MOD09GA FCC 01/09/2007 RGB-721,  
964 UTM 34S WGS84). Blue crosses indicate the field plot distribution (section 2.2), while red crosses show the  
965 locations of the training samples used in the land cover classification (section 3.1).

966

967

968

969

970

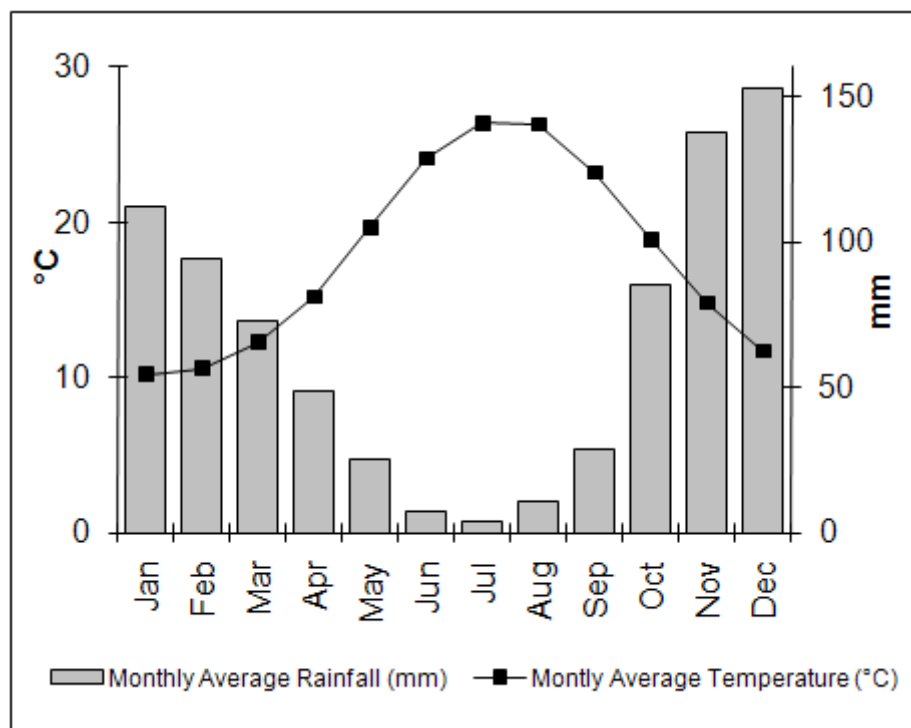


Figure 3. Ombrothermic diagram of the Kalamata (Peloponnese, Greece) meteorological station (37°41" N 22°11" E) 1956-1997 (Hellenic National Meteorological Service, [www.hnms.gr](http://www.hnms.gr)).

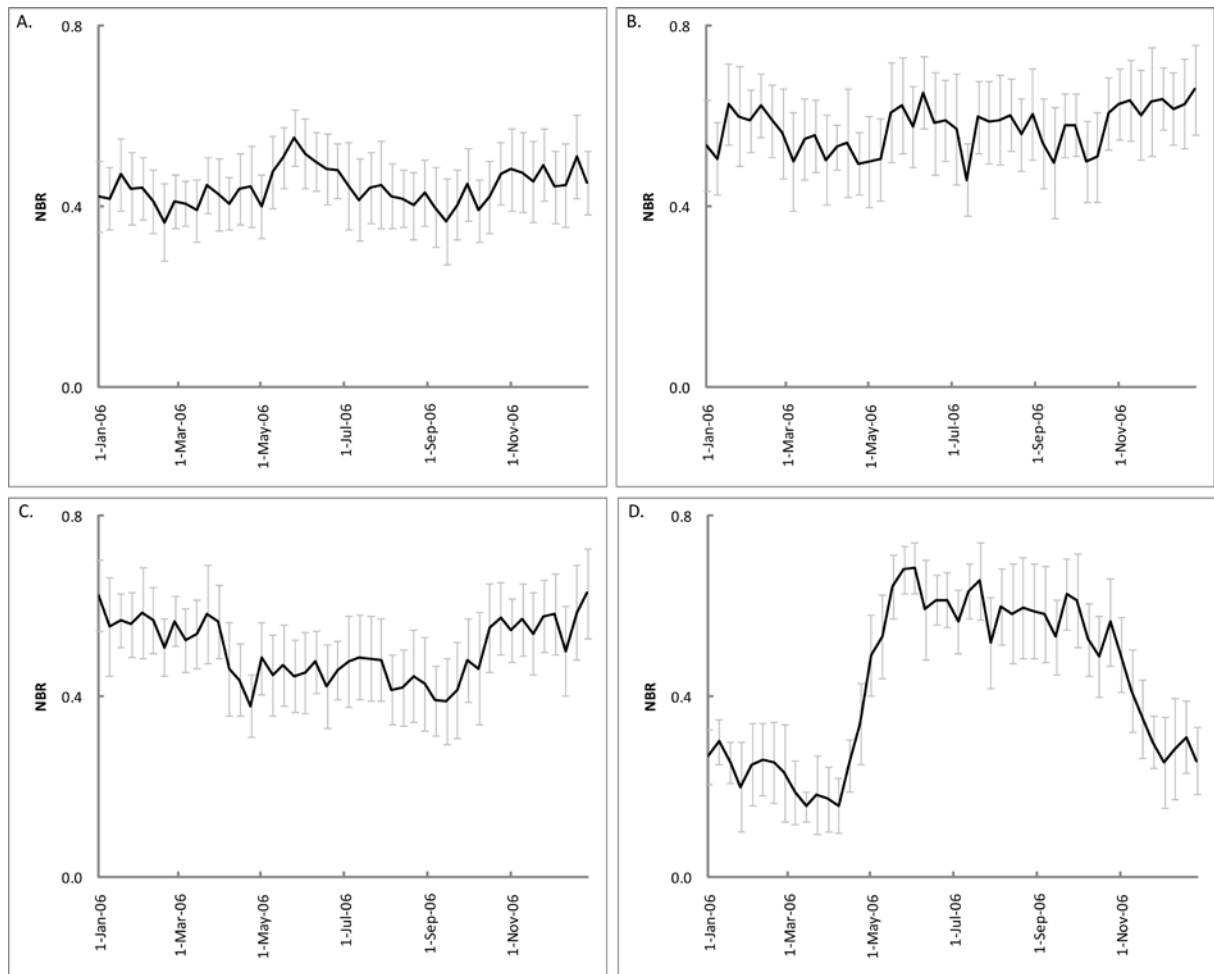


Figure 4. Mean temporal profile ( $\pm$  sd) of (A) shrub land, (B) coniferous forest, (C) olive groves and (D) deciduous forest training samples used in the pre-fire land cover classification.

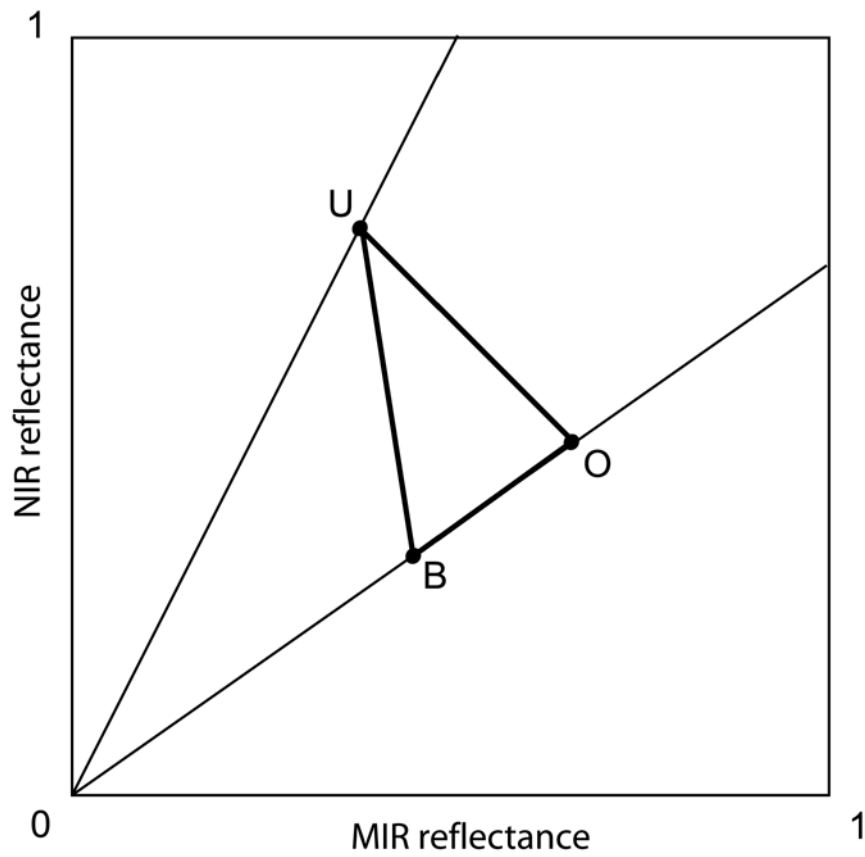


Figure 5. Example pre/post-fire trajectory of a pixel in the MIR-NIR feature space. A pixel displaces from unburned (U) to burned (B). O resembles the position of an optimally sensed burned pixel. The dNBR is sensitive to the displacement  $|UO|$  and insensitive to the displacement  $|OB|$ .

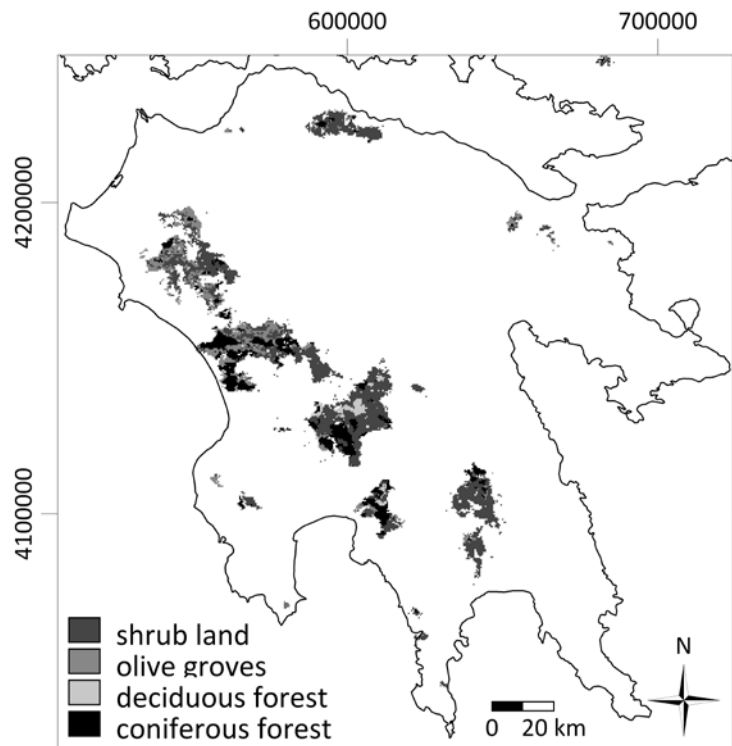


Figure 6. Pre-fire land cover map obtained after performing a maximum likelihood classification on a MODIS NBR time series of the pre-fire year 2006 (temporal profiles of training samples are given in figure 4).

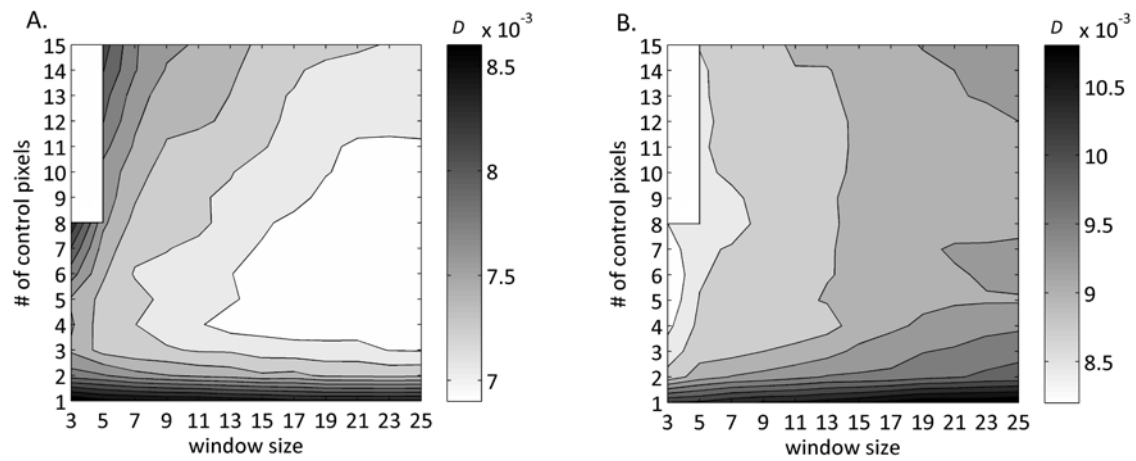


Figure 7. Median dissimilarity  $D$  of the 500 sample pixels in function of varying number of control pixels and window size for (A) a pre-fire year and for (B) a post-fire year. For the post-fire year, the same control pixels setting as in the pre-fire year is preserved. The grayscale reflects the temporal similarity, while the white areas in the upper-left corner represent impossible combinations (number of control pixels  $> 8$ , for  $3 \times 3$  window size).

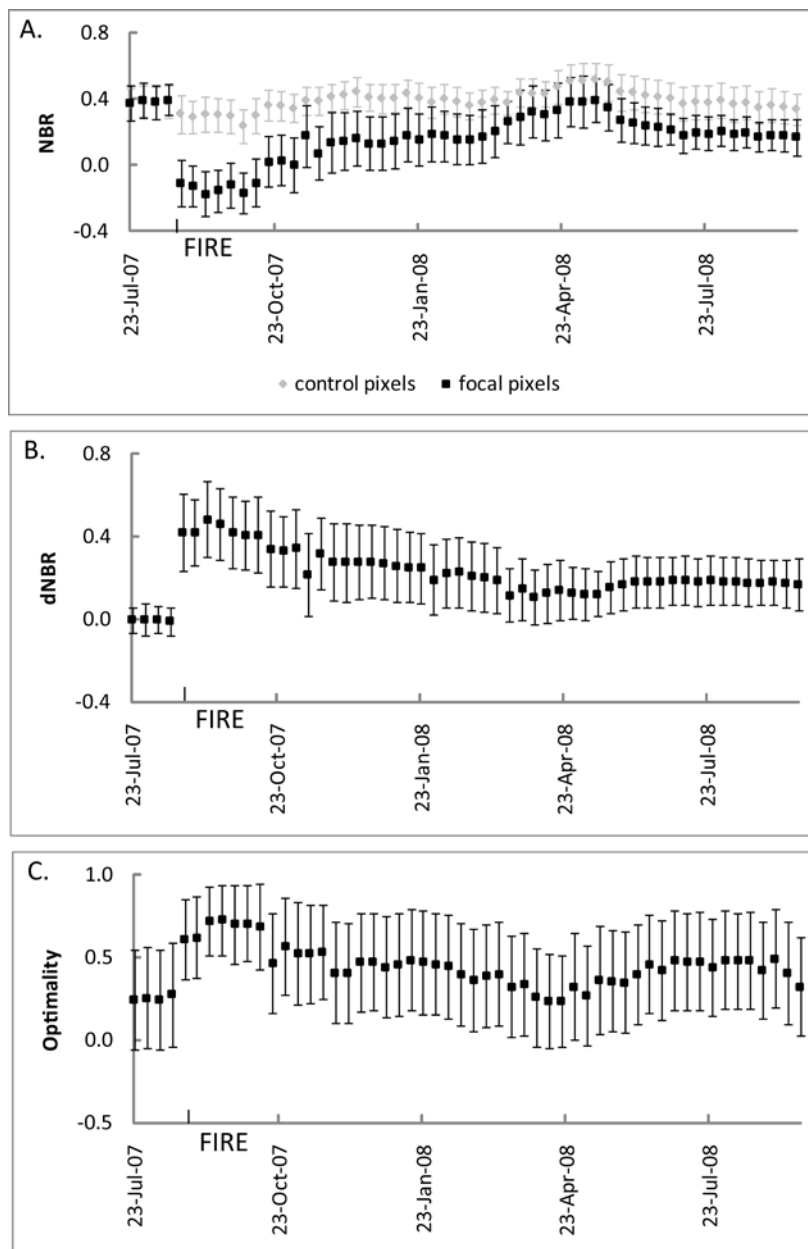


Figure 8. Time series of (A) mean NBR of control and focal pixels, (B) mean dNBR and (C) mean optimality (C) shrub land pixels before the fire event. The vertical bars indicate the sd.



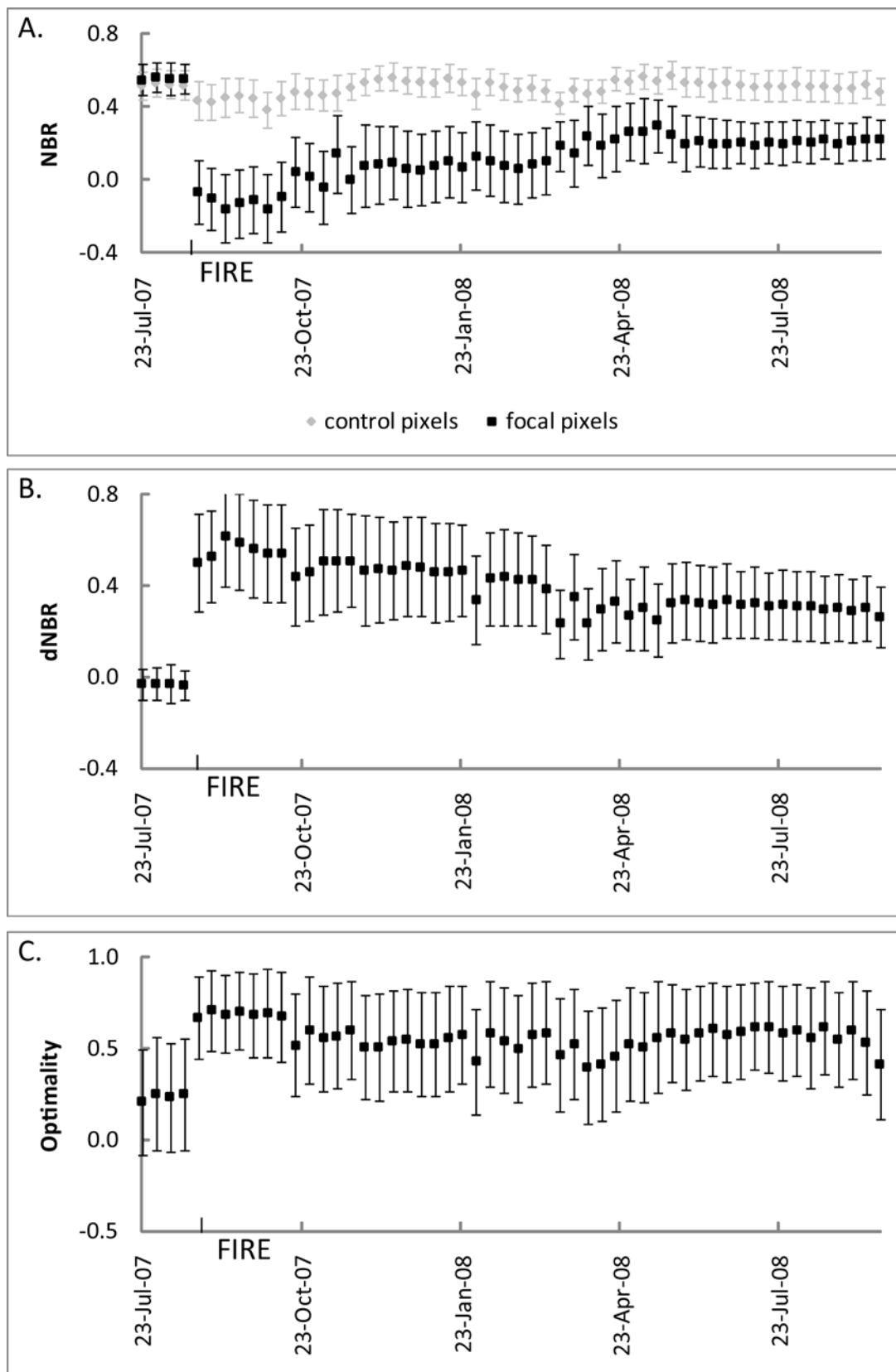


Figure 9. Time series of (A) mean NBR of control and focal pixels, (B) mean dNBR and (C) mean optimality (C) coniferous forest pixels before the fire event. The vertical bars indicate the sd.

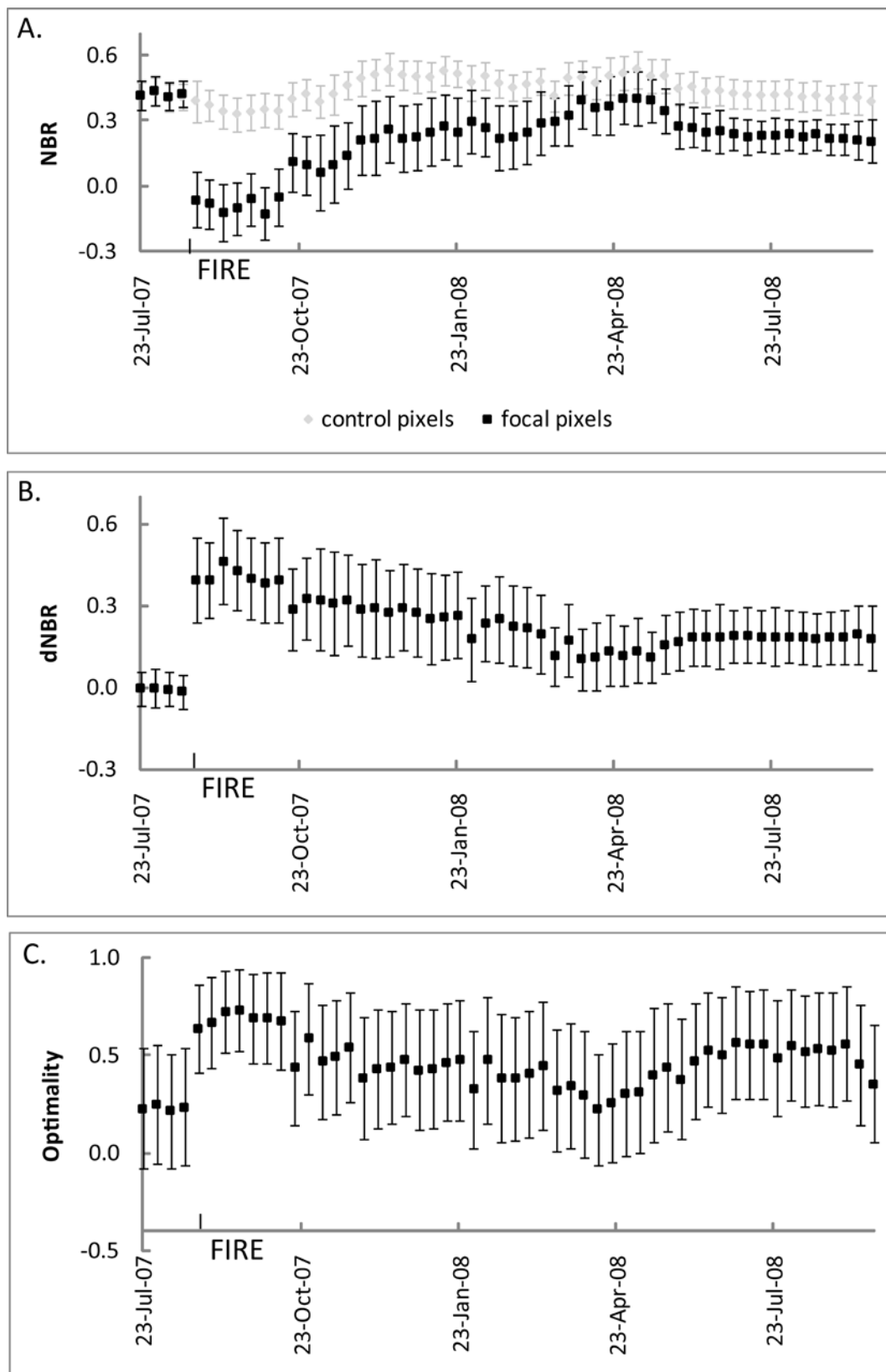


Figure 10. Time series of (A) mean NBR of control and focal pixels, (B) mean dNBR and (C) mean optimality (C) olive groves pixels before the fire event. The vertical bars indicate the sd.

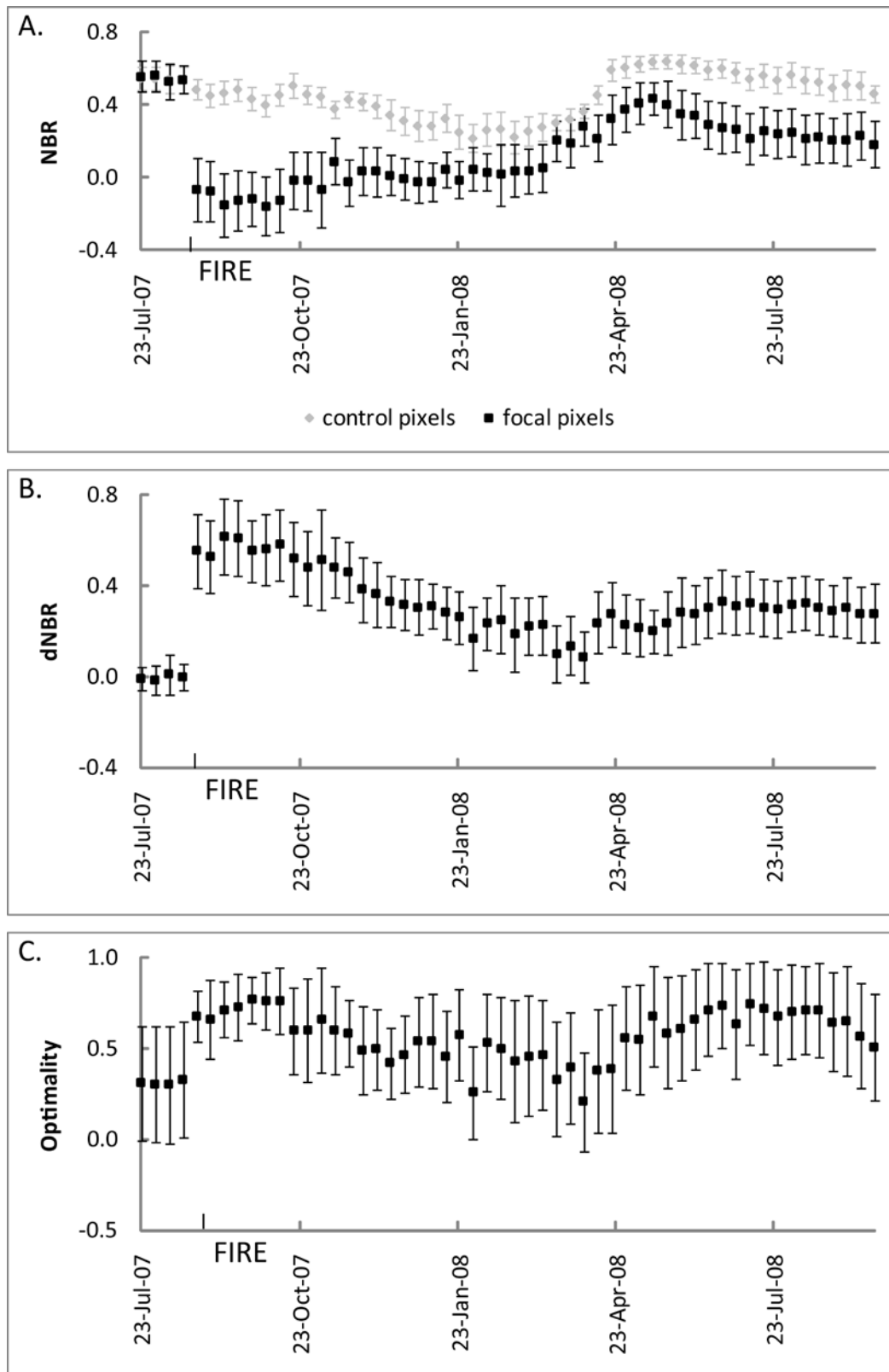


Figure 11. Time series of (A) mean NBR of control and focal pixels, (B) mean dNBR and (C) mean optimality (C) deciduous forest pixels before the fire event. The vertical bars indicate the sd.

1016 Table 1. GeoCBI criteria used to estimate fire/burn severity in the field (after De Santis and Chuvieco 2009).

Stratum	Burn severity scale						
	No effect	Low		Moderate		High	
	0	0.5	1	1.5	2	2.5	3
Substrates	FCOV						
Litter (l)/light fuel (lf) consumed	0 %	--	50 % 1	--	100 % 1	> 80 % lf	98 % lf
duff	0 %	--	Light char	--	50 %	--	Consumed
Medium/heavy fuel	0 %	--	20 %	--	40 %	--	> 60 %
Soil & rock cover/color	0 %	--	10 %	--	40 %	--	> 80 %
Herbs, low shrubs and trees less than 1 m	FCOV						
% Foliage altered	0 %	--	30 %	--	80 %	95 %	100 %
Frequency % living	100 %	--	90 %	--	50 %	< 20 %	0 %
New sprouts	Abundant	--	Moderate-high	--	Moderate	--	Low-none
Tall shrubs and trees 1 to 5 m	FCOV						
% Foliage altered	0 %	--	20 %	--	60-90 %	> 95 %	branch loss
Frequency % living	100 %	--	90 %	--	30 %	< 15 %	< 1 %
LAI change %	0 %	--	15 %	--	70 %	90 %	100 %
Intermediate trees 5 to 20 m	FCOV						
% Green (unaltered)	100 %	--	80 %	--	40 %	< 10 %	none
% Black/brown	0 %	--	20 %	--	60-90 %	> 95 %	branch loss
Frequency % living	100 %	--	90 %	--	30 %	< 15 %	< 1 %
LAI change %	0 %	--	15 %	--	70 %	90 %	100 %
Char height	none	--	1.5 m	--	2.8 m	--	> 5 m
Big trees >20 m	FCOV						
% Green (unaltered)	100 %	--	80 %	--	50 %	< 10 %	none
% Black/brown	0 %	--	20 %	--	60-90 %	> 95 %	branch loss
Frequency % living	100 %	--	90 %	--	30 %	< 15 %	< 1 %
LAI change %	0 %	--	15 %	--	70 %	90 %	100 %
Char height	none	--	1.8 m	--	4 m	--	> 7 m

1017

1018 Table 2. Error matrix of the pre-fire land cover map (accuracy verified based on 150 reference points)

		Reference data				User's accuracy
		S	O	D	C	
Classified data	S	47	5	1	10	0.75
	O	3	9	1	6	0.47
	D	1	0	13	0	0.93
	C	12	0	1	41	0.76
Producer's accuracy		0.75	0.64	0.81	0.72	<b>0.73</b>
		Kappa				<b>0.60</b>

1019

1020

1021 Table 3. Descriptive dNBR and optimality statistics of the TM and MODIS IA and EA

	TM		MODIS	
	IA	EA	IA	EA
Mean dNBR ( $\pm$ sd)	0.56 (0.29)	0.29 (0.19)	0.44 (0.19)	0.21 (0.14)
Mean optimality ( $\pm$ sd)	0.65 (0.25)	0.47 (0.29)	0.68 (0.24)	0.50 (0.30)

1022 Table 4. Linear regression results between on the one hand GeoCBI field data and  $\text{dNBR}_{\text{TM}}$ , on the other  
 1023 between downsampled  $\text{dNBR}_{\text{TM}}$  and  $\text{dNBR}_{\text{MODIS}}$  in both IA and EA schemes ( $n = 150$ ,  $p < 0.001$ ).

Model form	a ( $\pm$ sd)	b ( $\pm$ sd)	R <sup>2</sup>
$\text{GeoCBI} = a \times \text{dNBR}_{\text{TM,IA}} + b$	0.649 (0.033)	1.455 (0.019)	0.72
$\text{GeoCBI} = a \times \text{dNBR}_{\text{TM,EA}} + b$	0.767 (0.056)	1.508 (0.018)	0.56
$\text{dNBR}_{\text{TM,IA}} = a \times \text{dNBR}_{\text{MODIS,IA}} + b$	0.067 (0.037)	0.804 (0.069)	0.59
$\text{dNBR}_{\text{TM,EA}} = a \times \text{dNBR}_{\text{MODIS,EA}} + b$	0.035 (0.022)	0.730 (0.082)	0.45

1024  
 1025